Structure-Property Relation of Trimethyl Ammonium Ionic Liquids for Battery Applications

Daniel Rauber [1,*][ID], Andreas Hofmann [2][ID], Frederik Philippi [3][ID], Christopher W. M. Kay [1,4][ID], Tatiana Zinkevich [5], Thomas Hanemann [2,6][ID] and Rolf Hempelmann [1]

[1] Department of Chemistry, Saarland University, Campus B2.2, 66123 Saarbrücken, Germany; christopher.kay@uni-saarland.de (C.W.M.K.); r.hempelmann@mx.uni-saarland.de (R.H.)

[2] Karlsruher Institut für Technologie (KIT), Institut für Angewandte Materialien–Werkstoffkunde (IAM-WK), Hermann-von-Helmholtz-Platz 1, 76344 Eggenstein-Leopoldshafen, Germany; andreas.hofmann2@kit.edu (A.H.); thomas.hanemann@kit.edu (T.H.)

[3] Department of Chemistry, Molecular Sciences Research Hub, White City Campus, Imperial College London, London W12 0BZ, UK; f.philippi18@imperial.ac.uk

[4] London Centre for Nanotechnology, University College London, 17-19 Gordon Street, London WC1H 0AH, UK

[5] Karlsruher Institut für Technologie (KIT), Institut für Angewandte Materialien—Energiespeichersysteme (IAM-ESS), Hermann-von-Helmholtz-Platz 1, 76344 Eggenstein-Leopoldshafen, Germany; tatiana.zinkevich@kit.edu

[6] Institut für Mikrosystemtechnik, Universität Freiburg, Georges-Köhler-Allee 102, 79110 Freiburg, Germany

[*] Correspondence: daniel.rauber@uni-saarland.de; Tel.: +49-681-302-64253

Featured Application: Rechargeable batteries.

Abstract: Ionic liquids are attractive and safe electrolytes for diverse electrochemical applications such as advanced rechargeable batteries with high energy densities. Their properties that are beneficial for energy storage and conversion include negligible vapor-pressure, intrinsic conductivity as well as high stability. To explore the suitability of a series of ionic liquids with small ammonium cations for potential battery applications, we investigated their thermal and transport properties. We studied the influence of the symmetrical imide-type anions bis(trifluoromethanesulfonyl)imide ($[TFSI]^-$) and bis(fluorosulfonyl)imide ($[FSI]^-$), side chain length and functionalization, as well as lithium salt content on the properties of the electrolytes. Many of the samples are liquid at ambient temperature, but their solidification temperatures show disparate behavior. The transport properties showed clear trends: the dynamics are accelerated for samples with the $[FSI]^-$ anion, shorter side chains, ether functionalization and lower amounts of lithium salts. Detailed insight was obtained from the diffusion coefficients of the different ions in the electrolytes, which revealed the formation of aggregates of lithium cations coordinated by anions. The ionic liquid electrolytes exhibit sufficient stability in NMC/Li half-cells at elevated temperatures with small current rates without the need of additional liquid electrolytes, although Li-plating was observed. Electrolytes containing $[TFSI]^-$ anions showed superior stability compared to those with $[FSI]^-$ anions in battery tests.

Keywords: ionic liquids; ammonium; batteries; electrolytes⁻

1. Introduction

Ionic liquids are organic salts that melt below ambient temperatures. They are well established as a class of liquid materials with an exceptional combination of favorable properties. General characteristics of ionic liquids include ultralow vapor-pressure, intrinsic electric conductivity, relatively high ionic concentration as well as high thermal, chemical and electrochemical stabilities. As result of these features, ionic liquids are in development or actually implemented in many technical applications ranging from small-scale niche uses to industrial processes on a production scale [1,2]. Besides offering a range of completely

novel processes, ionic liquids are also used to improve existing techniques, for instance, in terms of safety, performance or durability. Many of the ionic liquids' technical implementations thereby lie in the field of electrochemical energy storage and conversion [3]. Research in this field is driven by the search for more efficient and safer devices in the context of defossilization and energy supply as the transformation to more sustainable societies accelerates.

Ionic liquids generally meet many of the criteria for advanced battery electrolytes by offering a broad electrochemical window and increased safety due to their high thermal stabilities, negligible volatility and low inflammability [4,5]. These molten salts often have high dissolution capacities for many compounds of different polarities, including conducting salts required for lithium, lithium ion and post-Li batteries. Using mixtures of ionic liquids and lithium salts increases the temperature range in which electrolytes can be employed. At lower temperatures a salting out of the Li-salts is often prevented by formation of eutectic mixtures, whereas at higher temperatures the operating range is extended due to extremely low vapor pressure. Commonly used salts for lithium batteries with high solubility in ionic liquids are lithium bis(trifluoromethanesulfonyl)imide (LiTFSI) and lithium bis(fluorosulfonyl)imide (LiFSI). Furthermore, the huge diversity of possible ionic liquid combinations and modifications offers adjustability towards particular desired properties. The main disadvantage of ionic liquids in comparison with commonly used electrolytes based on molecular solvents, such as dialkyl carbonates, is their lower ionic conductivity as a result of the strong, long-ranging Coulombic forces that retard the liquid dynamics [6,7]. Therefore, batteries using undiluted ionic liquid electrolytes are limited in their cycling rates or must be operated at elevated temperatures. However, the lower charge and discharge rate improves the stability and durability of the battery, thus ionic liquid electrolytes are promising for stationary uses. Using large-scale stationary batteries is regarded as essential to back up the power grid in the future. The demand for these energy storage devices results from the increased use of renewable energy—a characteristic of which is the discontinuous generation of energy. Molecular solvents can be used as additives in ionic liquid electrolytes to increase conductivity, thus providing electrolytes with well-balanced liquid range, safety and performance [8]. Nevertheless, one of the main advantages resulting from the use of undiluted ionic liquids—the significantly increased thermal stability—is thereby partially reduced [9]. It is also possible to use ionic liquids as plasticizers in polymer-electrolytes to improve lithium ion diffusion in this type of battery while preserving benefits of gelled electrolytes, for instance, in the manufacturing process [10].

Ionic liquids based on ammonium cations have a number of benefits. These include high thermal stability as well as commercial availability of a large range of different amine precursors that are cost-efficient and facile in handling, contrary to the phosphines necessary in the synthesis of phosphonium-based ionic liquids. In addition, the electrochemical stability of ammonium cations is among the highest reported and usually significantly higher than for ionic liquids based on the more common imidazolium cation. Hence, quaternary ammonium cations are also stable at the harsh cathodic conditions of the reactive lithium metal, which is usually not the case for organic electrolytes [11]. The anions [FSI]⁻ and [TFSI]⁻ result in ionic liquids with a combination of excellent properties for the use as electrolytes [12]. Ionic liquid incorporating the [FSI]⁻ anion in general show higher fluidities, lower temperatures of solidification [13] and formation of a robust solid-electrolyte interphase (SEI) [14], whereas the [TFSI]⁻ based molten salts have higher thermal and electrochemical stabilities. Although [TFSI]⁻ ionic liquids have slower transport properties than the [FSI]⁻ ones with the same cation, they still have lower viscosities and higher conductivities than most ionic liquids with the same cation, but other anions [15]. Some benefits of the two anions can be combined using the asymmetric (fluorosulfonyl)(trifluormethylsulfony)imide anion [13]. However, this anion is currently only sparsely commercialized.

Among the most widespread and mature battery technologies are those based on lithium [16]. These batteries combine high energy densities, high power and low weight with longevity and flexibility in shape and size. Rechargeable batteries based on lithium are the dominant type of energy storage devices for portable electronics and in the field of electric mobility. Lithium batteries and lithium-ion batteries contain an electrolyte in liquid state which is able to transport lithium ions between the electrodes. Commercial lithium batteries containing lithium electrodes are used as primary (non-rechargeable) batteries since depositing and re-dissolving lithium from the electrolyte forms dendrites on the lithium surface as result of repeated charging and discharging [17]. The growth of these dendrites may result in short-circuiting of the battery resulting in thermal runaway [18]. However, rechargeable batteries based on lithium metal remain attractive due the extremely high specific capacity and lowest electrochemical potential allowing high amounts of energy to be stored [19]. Furthermore, lithium-ion batteries, which—with correct use—do not suffer from lithium dendrite formation, are close to their theoretical capacity, making the use of still unknown alternative anode materials inevitable if the energy density is to be increased [20]. By simply adjusting the composition and properties of the electrolyte the formation of dendrites may be sufficiently suppressed [21].

Another problem is the thermodynamic instability of many electrolytes towards metallic lithium resulting in parasitic reactions and low cycle stability [22]. The main disadvantages of batteries using liquid electrolytes are concerns in terms of safety due to the use of highly flammable organic solvents and lithium salts with low thermal stability in the electrolyte. A further method for the increase of energy density in lithium-based batteries is the use of high voltage cathode materials. The use of high voltage cathode materials in turn demands electrolytes with increased electrochemical stabilities [23]. These different factors show that the optimization of the electrolyte is an important factor in the search for rechargeable batteries with increased energy density, cycle-stability and safety. Therefore, research into the characteristics of novel electrolyte systems for existing, established battery technologies also have implications on the search for advanced electrolytes to be used in potential batteries utilizing new cell chemistries.

Here, we have studied the use of quaternary, aprotic ammonium ionic liquids as potential electrolytes for lithium batteries. We focused on the use of small cations based on trimethyl ammonium with the generalized formula $[N111X]^+$, with X being an alkyl or ether functionalized side chain, and imide based anions, namely $[TFSI]^-$ and $[FSI]^-$. We investigated the thermal transitions at low temperatures and the transport properties of the pure ionic liquids and corresponding lithium solutions made from lithium salts with the same anion. Besides the effects related to the ion structures, we also examined the change in properties upon addition of lithium salt in 0.25 molar concentration for all and a concentration of 1.5 M [Li][TFSI] for two selected ionic liquids. Additionally, we investigated the electrochemical stability of the mixtures and with respect to their use in Li based half-cells.

2. Materials and Methods

2.1. Synthesis of the Ionic Liquids

The ionic liquids investigated in this work were prepared by alkylation of the amine and subsequent anion exchange. In the first step, an aqueous solution of trimethylamine was reacted with either alkyl-bromide or alkyl-ether-bromide to obtain the corresponding aprotic ammonium bromide salt. The high melting salts obtained were dissolved in water and the bromide anion exchanged with an imide anion by metathesis with an alkali metal salt of bis(fluorosulfonyl)imide or bis(trifluoromethanesulfonyl)imide. The resulting ionic liquids were further purified and dried in high vacuum. Identity and purity of the samples were confirmed by multinuclear NMR-spectroscopy. Absence of halides was confirmed by testing with $AgNO_3$-solution. Water content after drying in oil pump vacuum for at least two days was below 100 ppm, as confirmed by Karl–Fischer-titration. Further details of the synthesis are given in the supporting information.

The ionic liquids prepared as described above were dried on a vacuum line for two days prior to each physicochemical measurement and handled using Schlenk techniques or a Labmaster 130 glove box (MBraun, Garching, Germany) with oxygen and water levels below 1 ppm. Mixtures of the ionic liquids with lithium salts were prepared by weighting the dried lithium salt for the electrolyte of the required concentration in a volumetric flask, adding a stir bar and filling with ionic liquid below the graduation. After stirring until complete dissolution of the lithium salt, the stir bar was removed, and the volumetric flask was filled to the graduation and shaken for several minutes. The binary mixtures prepared this way were then degassed and dried again for two days and handled under inert conditions.

2.2. Thermal Transitions

Thermal behavior of the samples in the solid and liquid range was investigated by differential scanning calorimetry using a DSC 1 STARe (Mettler Toledo, Gieβen, Germany) with a liquid nitrogen cooling system. Hermetically sealed samples for the DSC measurements of about 10 mg ionic liquid or lithium solution in aluminum crucibles were prepared in the glove box. Comparably slow scan rates of $\pm 1\ ^\circ C\ min^{-1}$ were applied to favor crystallization of the samples upon cooling (preventing the samples from quenching) and to obtain more accurate glass transition temperatures. In a first dynamic step, the samples were heated with $+10\ ^\circ C\ min^{-1}$ to 120 $^\circ C$ to obtain an isotropic liquids state. The samples were cooled to $-120\ ^\circ C$ afterwards with a cooling rate of $-1\ ^\circ C\ min^{-1}$. All samples either crystallized or vitrified during the course of the cooling. Afterwards, the samples were heated to 120 $^\circ C$ with a heating rate of $+1\ ^\circ C\ min^{-1}$. First order phase transitions (melting point, crystallization point and solid–solid transitions) are reported as the peak maximum, while the glass transitions were determined by the midpoint method.

2.3. Density

The density was obtained by a precision densitometer from Anton Paar (DMA4500M) in a temperature range between 15 $^\circ C$–90 $^\circ C$ provided that the mixtures in this range were liquid. Otherwise, a smaller range was used (if samples did not remain in liquid state for sufficient time). Mixtures were taken inside the glovebox in a syringe (2 mL) and immediately injected into the device without any air contact. The standard uncertainty of the temperature during the measurement was $u(T) = 0.01\ ^\circ C$.

2.4. Viscosity

The temperature dependent dynamic viscosities were determined using a MCR 301 rheometer (Anton Paar, Graz, Austria) with a cone-plate setup on a vibration-isolated table. The cone used was a CP50-1 with 49.95 mm diameter and a cone angle of 1°. The gap size between the cone tip and plate was 0.101 mm. The rheometer was calibrated using a general viscosity standard with nominal viscosity of 129 mPa s (Paragon scientific, Prenton, UK). All measurements were conducted under flow of dry nitrogen to avoid the uptake of moisture. For the investigation of the *T*-dependence, viscosity values from 25 to 100 $^\circ C$ were measured in 5 $^\circ C$ steps. Prior to each measurement, the temperature was allowed to equilibrate for at least 20 min with deviation less than $\pm 0.01\ ^\circ C$ during the measurements. For each temperature, the shear-dependent viscosity was recorded for shear-rate values ranging from $5\ s^{-1}$ to $80\ s^{-1}$.

2.5. Conductivity

Temperature-dependent specific conductivities of the ionic liquids and lithium salt solutions were determined by impedance spectroscopy with an SP-150 potentiostat (Biologic, Seysinnet-Pariset, France). The conductivity probe (WTW, Weilheim, Germany) consisted of two rectangular, platinized platinum electrodes fused into glass and had a nominal cell constant of 0.5 cm^{-1}. The actual cell constant was determined using commercial conductivity standards. The samples were sealed in the conductivity cell and placed in a Proline

RP 1845 thermostat (LAUDA, Lauda-Königshofen, Germany) with T-stability of $\pm 0.01\ °C$. The temperature-dependent measurements were performed from 85 °C to 10 °C in steps of 5 °C. For each temperature, three impedance spectra with applied voltages of 5, 10 and 15 mV were recorded in the frequency range from 200 kHz to 1 Hz in 50 logarithmic steps. The resistance of the electrolytes, R, determined this way were averaged with a deviation of about $\pm 1\%$. The specific conductivity κ was calculated from the cell constant k divided by the determined resistance R. Molar conductivities were calculated using Equation (1):

$$\Lambda_{\mathrm{M}} = \frac{\kappa\, M}{\rho} \tag{1}$$

with M being the molar mass of the mass of the ionic component, weighted with the stochiometric coefficients in case of the salt mixtures.

2.6. Self-Diffusion Coefficients

^{1}H, ^{19}F and ^{7}Li pulsed-field gradient self-diffusion coefficient measurements were carried out on a Bruker NMR spectrometer serving at a ^{1}H Larmor frequency of 300 MHz. Samples were prepared in an argon filled glove box (see Section 2.8) by filling the mixtures in Hilgenberg tubes (glass no. 14, order no. 4007410) with outer diameter of 1.0 mm, which were placed inside of a standard NMR tube (closed by screw cap). A stimulated-echo pulse sequence with bipolar gradients was used to perform all measurements. The diffusion time Δ and the gradient duration δ were 100 ms and 3 ms, respectively. The preliminary T_1 experiments allowed us to estimate the relaxation time and to set a recycling delay of $5 \cdot T_1$. The number of scans was optimized for each experiment to provide a good signal-to-noise ratio. To ensure that the measured diffusion coefficients are free from a convectional contribution, the experiments at the highest accessible temperature were carried out with a set of different diffusion times ranging from 30 to 300 ms. The similarity of the resultant values proved a negligible effect. All diffusion curves of the diffusing species i represented a single Gaussian function, and the diffusion coefficient $D_{\mathrm{S}}(i)$ was determined from the Stejskal–Tanner Equation (2):

$$I(t) \propto I_0 \exp\left(-D_{\mathrm{S}}(i)\, \gamma^2 g^2 \delta^2 \left(\Delta - \frac{\delta}{3}\right)\right) \tag{2}$$

where $I(t)$ is the signal intensity after a time t, I_0 is the intensity of the signal in the absence of gradient pulse, γ denotes the gyromagnetic ratio of the investigated nucleus, g is the gradient strength, and Δ and δ are the diffusion time and the gradient duration, respectively.

2.7. Fitting of the Transport Properties

Transport properties of the pure ionic liquids and the mixtures with lithium salts were fitted with the Vogel–Fulcher–Tammann–(Hesse) (VFT) Equation (3), which is commonly applied to describe the transport properties of fragile glass-forming materials in dependence on temperature [24]. The VFT equation is frequently used and describes the temperature-dependence of the ionic liquid transport properties in a broad temperature range more accurately than the Arrhenius Equation (4) [25,26].

$$Y = Y_0 \exp\left(\frac{B_Y}{T - T_{0,Y}}\right) \tag{3}$$

The variable Y being the fitted transport property, e.g., the dynamic viscosity η, the specific conductivity κ, the molar conductivity Λ_{M} or the self-diffusion coefficients $D_{\mathrm{S}}(i)$ (with i being ionic liquid cation (^{1}H), anion (^{19}F) or lithium cation (^{7}Li)). Y_0, B_Y and $T_{0,Y}$ (the so-called Vogel temperature) are material dependent fitting parameters. The parameter B_Y obtains positive values for $Y = \eta$ and negative values for $Y = \kappa, \Lambda_{\mathrm{M}}, D_{\mathrm{S}}(i)$. Angell's strength parameter δ_Y is the absolute value of B_Y divided by $T_{0,Y}$ and is a measure of the

liquid fragility of glass formers, and thus describes the rate of change in a transport property upon change in temperature. δ_Y is often referred to as D in the literature, which is avoided here in order to prevent confusion with the self-diffusion coefficients $D_S(i)$ [27]. Angell's strength parameter is related to the kinetic fragility index m, an alternative measure for liquid fragility, by the relation $m = 16 + 590\,\delta_Y^{-1}$ [27]. Liquids classified as 'fragile' show fast changes in the transport properties and narrow glass transition temperature range, while 'strong' glass forming liquids have nearly constant activation energy of the transport process and broad temperature intervals of the glass transition. Notwithstanding the more accurate description of the T-dependence of the ionic liquid transport properties by the VFT Equation (2) in a broad temperature range, the Arrhenius Equation (4) can be used to determine the activation energy $E_{a,Y}$ of a transport process in a narrower temperature range, where linear fits are feasible and the activation energy can be regarded as constant [28].

$$\ln(Y) = \ln(Y_0) - \frac{E_{a,Y}}{RT} \tag{4}$$

where $E_{a,Y}$ is the activation energy of the transport quantity Y within the considered temperature interval. For $Y = \eta$, positive values of $E_{a,Y}$ are obtained, while $Y = \kappa, \Lambda_M, D_S(i)$ yields negative values.

2.8. Electrochemistry

Electrolyte handling was performed in an argon-filled glove box (MBraun GmbH) with oxygen and water levels below 0.5 ppm. The cyclic voltammetry was carried out at a Zahner X-Pot potentiostat. Briefly, three electrode cells (EL-Cell GmbH, Hamburg, Germany) were measured with Li (Ø = 17 mm) (reference/counter electrode), platinum (Ø = 18 mm) (working electrode) and a glass fiber separator (Whatman, QMA, Ø = 19 mm) including electrolyte (volume: 75 µL) in between. The potential range was set to 3–6.5 V vs. Li/Li$^+$, and a scan speed of 1 mV·s^{-1} was used. To determine cell performance and cell pressure, a PAT-press system from EL-Cells was used with a potentiostat from Zahner (X-Pot). Electrode sheets (NMC (LiNi$_{0.33}$Mn$_{0.33}$Co$_{0.33}$O$_2$), d = 18 mm and lithium metal, d = 18 mm) and a QMA glass fiber separator (d = 21 mm) as well as 130 µL electrolyte were used in the cell. The cell was operated in a temperature chamber at T = 60 °C between 3.0 V and 4.3 V vs. Li/Li$^+$.

2.9. IR Spectroscopy

IR spectra were recorded with a Nicolet iS5 device inside of a glovebox (see 2.8 for glovebox conditions). An iD7 ATR unit with a diamond crystal was used for data acquisition. Omnic 9 was used for data analysis and spectra design. Measurement were performed by pasting small amounts of liquid (without pressure) or solid material (including pressure) onto the ATR crystal.

3. Results and Discussion

3.1. Molecular Structure, Thermal Properties and Density

The cations contain the generalized formula [N111X]$^+$, with X being an alkyl or ether functionalized side chain. The anions are either bis(fluorosulfonyl)imide ([FSI]$^-$) or bis(trifluoromethanesulfonyl)imide ([TFSI]$^-$). Molecular structures and abbreviations are shown in Figure 1.

Small cations were chosen since they usually show faster dynamics in liquid state [13]. The side-chain functionalization with ether groups was selected since this was reported to speed up the dynamics of ionic liquids, leading to faster ion transport [4]. The use of ammonium ionic liquids with the incorporation of an ether functionalization into the cation and the use of the [FSI]$^-$ anion was motivated by beneficial effects for the electrolyte dynamics, e.g., lower viscosity and higher conductivity. The dissolution of lithium salt in the ionic liquids always decreases the solidification temperature, whereas concomitantly, the dynamics become slower.
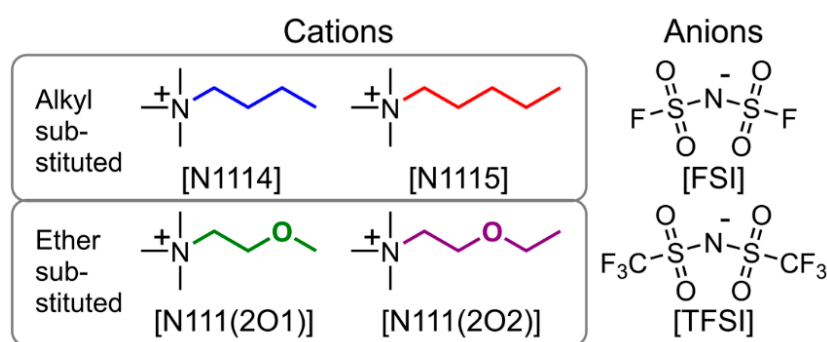
Cations　　　　　　　　　　　　　　**Anions**

Alkyl substituted: [N1114] [N1115]　[FSI]

Ether substituted: [N111(2O1)] [N111(2O2)]　[TFSI]

Figure 1. Molecular structures of the ionic liquids' ions and their abbreviations.

The solidification of an electrolyte marks the lower limit in which an electrochemical device can be operated and is therefore an essential characteristic. Solidification can either be in the form of a crystalline, ordered solid (crystallization) or amorphous glass (vitrification). For most applications, the use of room temperature ionic liquids, hence compounds with melting points below 25 °C, are of interest to ensure reliability and ease of operation. The thermal transitions of the ionic liquids in this study were investigated using differential scanning calorimetry (DSC) with slow scan rates to avoid quenching of the samples. The same program was used for all samples to ensure the comparability of glass formation and supercooling. It should be noted that the observed thermal transitions are always dependent on the experimental conditions such as heating rate, sample pre-treatment or crucible material. We are mainly interested in the solidification of the electrolytes as their lower application limit, further experiments, e.g., using different heating rates, are beyond the scope of this work. The obtained thermal transitions and densities of the quaternary ammonium ionic liquids and their mixtures with lithium salts are given in Table 1. Density values at other temperatures are given in the supporting information.

Table 1. Thermal transitions of the pure ionic liquids and Li-salt mixtures obtained by DSC at ± 1 °C min^{-1} scanning rates in closed Al-crucibles and their densities at 25 °C. Thermal transitions include crystallization temperatures T_c upon cooling, glass transition points T_g, cold crystallization temperatures T_{cc}, (transition from glassy to crystalline upon heating), transition temperatures for the change of crystalline phases T_{ss} and the melting temperatures T_m. Uncertainty in the temperatures is ± 1 °C.

Ionic Liquid	Lithium Salt c/mol·dm^{-3}	T_c [a]/°C	T_g/°C	T_{cc} [b]/°C	T_{ss}/°C	T_m [a]/°C	$\rho^{25\,°C}$/g mL^{-1}
[N1114][TFSI]	-	−30	-	-	−103 [a]; −100 [b]; −38 [b] 9 [b]	18	1.3919
[N1114][TFSI]	0.25	-	−78	−25	-	9	1.4173
[N1114][TFSI]	1.5	-	−48	−15	-	19	1.5268
[N111(2O1)][TFSI]	-	−17	-	-	-	38	−[c]
[N111(2O1)][TFSI]	0.25	−36	-	-	-	36	−[c]
[N111(2O1)][TFSI]	1.5	-	−56	-	-	-	1.5725
[N1114][FSI]	-	−18	-	-	−34 [a]; −35 [b] 9 [b]	22	1.3028
[N1114][FSI]	0.25	−30	-	-	−32 [a]; −28 [b]; 8 [b]	15	1.3186
[N111(2O1)][FSI]	-	12	-	-	-	34	−[c]
[N111(2O1)][FSI]	0.25	−18	-	-	−33 [a]; −28 [b] 9 [b]	18	1.3914
[N1115][TFSI]	-	−17	-	-	−2 [b]; 19 [b]	29	1.3638
[N1115][TFSI]	0.25	-	−72	−48	−8 [b]; 8 [b]	17	1.3854
[N111(2O2)][TFSI]	-	-	−83	−66	−55 [b]	0	1.4141
[N111(2O2)][TFSI]	0.25	-	−79	−18	-	−3	1.4341

[a] Observed in the cooling step (-1 °C min^{-1}); [b] observed in the heating step ($+1$ °C min^{-1}); [c] no sufficient supercooling to obtain a liquid at 25 °C.

Types of thermal behavior/DSC curves: The samples show a diverse and complex phase transition behavior, notwithstanding the similarity of their molecular structures. The low temperature molten salts can be classified according to their solidification behavior in

the cooling and heating traces. This results in three different types that are commonly observed [29]. The first type is characterized by the complete absence of ordered crystalline structures leading only to the formation of amorphous glasses at the glass transition temperature T_g. Samples of the second type show crystallization T_c upon cooling and melting T_m upon heating similar to the situation for most organic salts. Ionic liquids that belong to the third type of thermal transition show a glass transition upon cooling, followed by cold crystallization T_{cc} from the supercooled liquid state in the heating cycle and subsequent melting.

Overview of the thermal behaviors: Most bulk ionic liquids and the mixtures with lower lithium salt content belong to the second type, showing crystallization upon cooling. The mixtures with high amount of lithium salt form glasses upon cooling. The sample with the alkylated [N1114]$^+$ cation and 1.5 M [Li][TFSI] shows an additional T_{cc} (third type). The mixture of 1.5 M LiNTf$_2$ in [N111(2O1)]$^+$ is the only sample where ordered solids could not be observed under the conditions explored. Glass transitions are only found for ionic liquids with the [TFSI]$^-$ anion. For the mixtures of ionic liquids with lithium salts the values for the crystallization and melting temperature are slightly lower than for the bulk liquids. The only exception is the mixture of [N1114][TFSI] with 1.5 M [Li][TFSI], which has a melting point that is 1 °C higher than the pure ionic liquid. The diverse transition behavior is also reported for a phosphonium ionic liquid with comparable cation structure and [FSI]$^-$ anion [30]. Upon increasing the concentration of [Li][FSI], the thermal behavior changes from the second type for the pure ionic liquid to the third type for samples with 0.5 and 1 M concentration, and finally results in a first type behavior for high lithium salt concentrations [30].

Influence of anions type and cation side chains: For the ionic liquids with the alkylated [N1114]$^+$ cation and their 0.25 M Li-salt mixtures, the melting points and crystallization temperatures (if present) are slightly lower for the samples with the [TFSI]$^-$ anion compared to the [FSI]$^-$ anion. However, the situation is different in case of the samples with [N111(2O1)]$^+$ cation. For the ionic liquids with this cation, the samples with the [FSI]$^-$ anion show slightly lower melting points, but higher crystallization temperatures than the [TFSI]$^-$ analogues. The values for the melting point and solid–solid transition of the pure [N1114][TFSI] are in good agreement with literature reports [31]. Elongation of the alkyl side chain from butyl to pentyl leads to an increase in the crystallization and melting points of roughly 10 °C. As a consequence, [N1115][TFSI] is the only sample with purely alkyl side chains, that is not a room temperature ionic liquid. For alkylated samples, the addition of lithium salt leads to a change in thermal behavior from the second to third type, so that only a glass transition is obtained in the cooling trace. The functionalization of the cation side chain with an ether group in γ-position leads to an increase in the melting temperatures compared to the case of the butyl side chain for both the [TFSI]$^-$ and [FSI]$^-$ anion. In case of the pentyl group, the substitution of the γ-methylene group by an oxygen leads results in a decrease of the melting point by nearly 30 °C, giving the lowest melting point among the pure ionic liquids in this set for [N111(2O2)][TFSI].

Supercooling of the samples: Supercooling, meaning the occurrence of a liquid state below the melting point of a compound for longer times, is a common finding in the field of ionic liquids [32,33]. All the samples showing a thermal behavior of the third type have a strong tendency for supercooling with a trend that is more pronounced for samples with the [TFSI]$^-$ anion and ether functionalized side chains. Furthermore, the samples with dissolved lithium salts showed stronger supercooling than the pure ionic liquids. For some samples, this kinetic hindrance of crystallization even leads to the non-existence of crystallization temperatures under these experimental conditions and the formation of glasses upon cooling, so that these samples fall into the first and third types of DSC traces. The lowest supercooling is found for the sample [N111(2O1)][FSI], showing only 22 °C difference between crystallization and melting, while [N111(2O1)][TFSI] with 0.25 M [Li][TFSI] has a difference of 72 °C between both transitions. Due to the pronounced

supercooling, many of the ionic liquids' physicochemical properties could also be measured in the liquid state below their melting point.

Solid–solid transitions: In addition to the above-mentioned thermal properties, many of the samples showed additional solid–solid transition in the DSC traces, whereby the greater variety of transitions is obtained upon heating. The solid–solid transitions can be found for all four types of cations and two types of anions investigated here. A similar variety of solid phases is also found for ionic liquids with small phosphonium cations and various anions [34], as well as other ammonium ionic liquids with the anions used here [35]. Potential applications of these ionic liquids and their mixtures are in the field of organic plastic crystals.

Summary and rationalization of the thermal behavior: These overall diverse, complex and hard to predict behavior of the thermal transitions for samples with similar structures highlights the need for a fine-tuning of the molecular structure to achieve ionic liquids with low solidification temperatures. This allows for batteries with expanded application ranges. The ionic liquids and mixture show no clear trend in the melting transition with the chosen anion, side chain length and functionalization, which is contrary to the situation found for transport properties (shown below). For instance, a common finding for ionic liquids with multiple ether substituents are significantly reduced melting temperatures and often occurrence of only glass transition when compared to the alkylated analogues [36,37]. The only overall tendency for the thermal transitions is that the mixtures of IL with 0.25 M lithium salt show lower melting and crystallization temperatures. Accordingly, the formation of binary electrolytes consisting of ionic liquids and lithium salt can be a valuable tool to increase the liquid range of battery electrolytes. The lowering of the melting point for ionic liquid–lithium salt mixtures is a common finding [38] and can be attributed to increasing disorder in the resulting mixed crystal leading to a lower difference in entropy between solid and liquid state, as found for eutectic systems [39]. The entropic contribution of the dissolved lithium salt also serves as an explanation why the supercooling and glass formation is less pronounced for the $[FSI]^-$ samples, as these have lower $[Li]^+$ contents compared to the $[TFSI]^-$ mixture. Furthermore, a trend for the increase in glass transitions temperature upon increasing lithium salt concentration was found in the literature and attributed to the stronger ion–ion interaction of the small, charge localized Li-cation with the anions [40]. In this set, the effect is observed for [N1114][TFSI] where the glass transition is raised from $-78\,^\circ$C for the 0.25 M sample to $-48\,^\circ$C for the 1.5 M sample. This increase in the T_g upon increase of $[Li]^+$ is directly coupled to the increase of viscosity, that will be discussed below, as these two properties are related to each other [41].

The density values of the ionic liquids and their mixtures, on the contrary, show clear trends, Figure 2. The density increases significantly for the same cation when $[FSI]^-$ is replaced by $[TFSI]^-$. In addition, a density increase is also observed upon replacing the methylene unit in the side chain by an oxygen atom. Elongation of the side chain again leads to a decrease of the densities. Thus, the densities of the ionic liquids increase with increasing content of sulfur and fluorine. Increasing densities upon exchange of $[FSI]^-$ with $[TFSI]^-$ and addition of lithium salt was found also for ionic liquid electrolytes based on the 1-ethyl-3-methyl imidazolium cation $[C_2C_1im]^+$. The significant change in densities between the ether and alkyl samples can be rationalized by a change in the cation conformation as the difference between the weight of the methylene group and the oxygen is too small to account for these relatively large differences. Change in cation conformations from a linear side chain arrangement of the alkyl groups to a kinked one for ether-cations with curling of the side chain around the cation is well known in the literature [37,42]. All temperature-dependent densities showed a linear behavior within the investigated T-range.
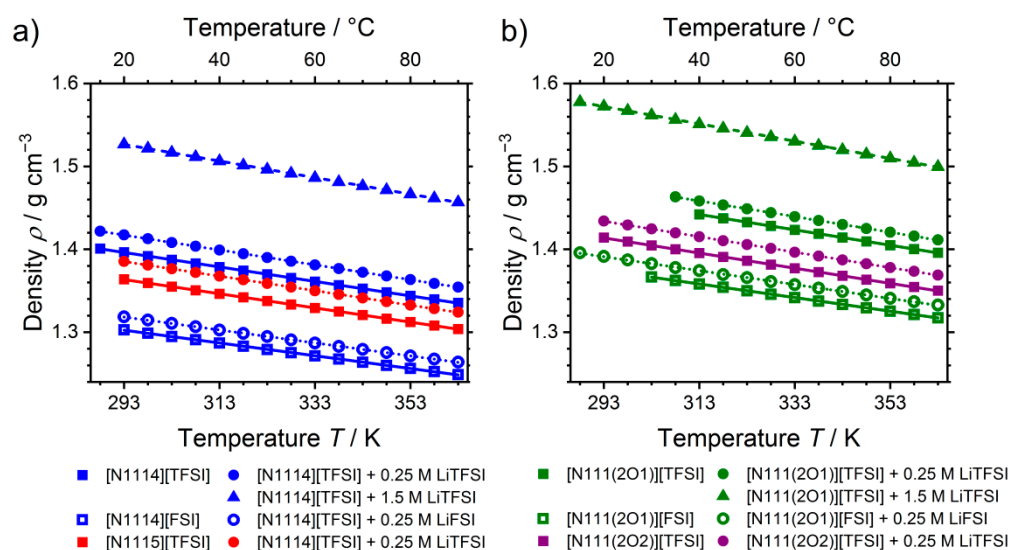
Figure 2. Temperature-dependent densities of the ionic liquids with (**a**) purely alkyl side groups and (**b**) ether functionalization in the side-chain.

3.2. Viscosity

Viscosity is one of the most important characteristics of ionic liquids since this class of materials suffers from the inherent disadvantage of slower dynamics compared to molecular fluids. Due to the presence of the strong, long-ranged Coulomb forces, low temperature molten salts have viscosity values that are at least one order of magnitude higher than conventional solvents and electrolytes. Decreasing the viscosity of ionic liquids is therefore a key aspect in the focused optimization of their properties. Critically, viscosity determines the transfer of the electroactive species in battery electrolytes and therefore limits the electrochemical reactions and charge/discharge rates. Beyond modification of the molecular structure of ionic liquids to achieve higher fluidities, a mixing of ionic and molecular liquids is another practical tool to achieve electrolytes with good transport properties. However, this approach to some extent comes at the cost of the advantages of pure ionic liquid electrolytes, such as negligible vapor pressure, increased safety and high chemical stability. The obtained viscosities of the ionic liquids at 25 °C, the fitting parameters following the VFT Equation (3), the Angell strength factor δ_η and activation energy $E_{a,\eta}$ obtained from the Arrhenius Equation (4) in the range of 25 to 60 °C are given in Table 2. Experimental viscosity values are given in the supporting information.

Table 2. Viscosity η of the pure ionic liquids and mixtures with lithium salts at 25 °C, VFT fitting parameters (η_0, B_η, $T_{0,\eta}$), Angell strength factor δ_η and activation energy $E_{a,\eta}$ (in the range of 25 to 60 °C) for the T-dependent viscosity.

Ionic Liquid	Li Salt c/mol·dm^{-3}	$\eta^{25\,°C}$/ mPa s	η_0/ 10^{-1} mPa s	B_η/K	$T_{0,\eta}$/K	δ_η	$E_{a,\eta}$/ kJ mol^{-1}
[N1114][TFSI]	-	99.2	1.772	784.9	174.1	4.51	32.9
[N1114][TFSI]	0.25	147.3	2.073	760.4	182.3	4.17	36.0
[N1114][TFSI]	1.5	1933	1.229	979.4	196.8	4.98	58.6
[N111(2O1)][TFSI]	-	59.6	2.805	632.7	180.1	3.51	29.0
[N111(2O1)][TFSI]	0.25	87.7	2.138	746.5	174.1	4.29	31.3
[N111(2O1)][TFSI]	1.5	833.9	1.675	926.5	189.3	4.89	48.9
[N1114][FSI]	-	55.1	2.053	835.4	148.8	5.61	25.1
[N1114][FSI]	0.25	62.0	2.183	819.7	153.1	5.35	25.9
[N111(2O1)][FSI]	-	38.9	1.996	800.9	146.3	5.47	23.3
[N111(2O1)][FSI]	0.25	45.5	4.502	550.0	178.8	3.08	24.7
[N1115][TFSI]	-	136.9	1.650	806.0	178.2	4.52	35.9

Table 2. *Cont.*

Ionic Liquid	Li Salt c/mol·dm^{-3}	$\eta^{25\,°C}$/ mPa s	η_0/ 10^{-1} mPa s	B_η/K	$T_{0,\eta}$/K	δ_η	$E_{a,\eta}$/ kJ mol^{-1}
[N1115][TFSI]	0.25	174.8	1.710	831.0	178.3	4.66	37.0
[N111(2O2)][TFSI]	-	57.8	2.116	731.9	167.7	4.36	28.1
[N111(2O2)][TFSI]	0.25	84.3	2.124	745.4	173.6	4.29	31.0

At 25 °C, the ionic liquids or their mixtures with lithium salt incorporating the [FSI]$^-$ have significantly lower viscosity values than the ones with the [TFSI]$^-$ anion and a common cation. The viscosity of the [TFSI]$^-$ samples are higher than those of [FSI]$^-$ ionic liquids by a factor of 1.80 for the [N1114]$^+$ cation and 1.53 for the [N111(2O1)]$^+$ cation. Elongation of the side chain from butyl to pentyl leads to an increase in viscosity by 38% for the alkylated sample, while for the ether-substituted samples, even a slight decrease is found (IL without salt). The largest effect on the viscosity is found for the side chain functionalization, and the ratio of alkyl to ether is more distinct for the [TFSI]$^-$ samples with values of 1.66 for the [N1114]$^+$/[N111(2O1)]$^+$ and 2.37 for the [N1115]$^+$/[N111(2O2)]$^+$ combination. For the [FSI]$^-$ samples, ether functionalization also reduces the viscosity significantly, but to a lower extent (1.42 for the [N1114]$^+$/[N111(2O1)]$^+$ pair). For all samples, the viscosity clearly increases upon addition of lithium salt. For the concentrated 1.5 M [Li][TFSI] samples, the raise in viscosity at 25 °C is distinct compared to the pure ionic liquids being 19.5 times the value for the alkylated [N1114][TFSI] and 14.0 times the value for the ether-ionic liquid [N111(2O1)][TFSI]. However, at 100 °C, the viscosity quotient between the concentrated solutions and the pure ionic liquid decreased to a factor 3.56 for the alkylated and 3.46 for the ether-substituted cation. Contrary to the sharp decrease in the viscosity ratio of lithium containing solution to pure ionic liquid in case of the 1.5 M samples, the ratio remains approximately constant for the samples with 0.25 M concentration. The *T*-dependence of all ionic liquids and their solutions could be well fitted with the VFT-equation (Figure 3). The values for the Angell strength factor are all in a quite narrow interval ranging from 3.05 to 5.61 and do not reveal a general trend. As the viscosities of the samples show no crossover with temperature, it is not surprisingly that the calculated activation energies for the viscous flow $E_{a,\eta}$ show the same trends as the viscosity values. In particular, a decrease in $E_{a,\eta}$ is observed upon replacing [TFSI]$^-$ by [FSI]$^-$, alkyl by ether side-chain, as well as for reducing the side-chain length and lithium content.

Factors governing the viscosity of the cation and anion are not independent of each other as seen by the difference in viscosity for the alkyl and ether substituted cation when exchanging the anion. Similar findings related to a coupling of cation and anion factors affecting the transport properties of ionic liquids are also found in other studies [37]. Lower viscosities for the liquids based on the [FSI]$^-$ anion than for ones based on [TFSI]$^-$ are a general finding [40] and might be attributed to the smaller ion size or the stronger interaction of the latter with the cation, as it was shown in the literature for the [C$_2$C$_1$im]$^+$ cation [43]. The increase in viscosity upon elongation of the side chain found for the alkylated sample can be understood in the strengthening of a liquid microstructure consisting of aggregated nonpolar hydrocarbon and polar ionic components [42,44]. In the case of 1-alkyl-3-methyl imidazolium [C$_x$C$_1$im][TFSI] ionic liquids, the clear emergence of this nanostructure is reported to occur when the side chain length is equal to or larger than pentyl (x ≥ 5) [45]. The underlying cause for the significantly lowered viscosity of the ether-substituted ionic liquids is the change in the cation conformation. While the side-chains of alkylated ionic liquids usually obtain linear conformation, the ether-groups are kinked and coordinate the positively charged part of the cation [37,42,46]. The origin for this curled structure is thought to be in the formation of intramolecular hydrogen bonding to the hydrogens in α-position to the cation center [47]. This curling of the ether chains leads to more spherical ions with better shielding of the positive charge and blocking of coordination sites at the cation. This shielding and blocking become more distinct for (slightly) longer

chains and reduces the overall interactions with the anion. In addition, the more polar ether-substituents suppress the formation of a nanostructure, which is contrary to less polar hydrocarbon groups. The combined effects of the altered cation conformation upon introduction of ether functionalities increases the fluidity of the ionic liquids drastically and gives an explanation why the viscosities of [N111(2O2)][TFSI] are even slightly lower than the ones with the shorter side chain, namely [N111(2O1)][TFSI]. Addition of lithium salts to ionic liquids raises their viscosities as a general finding [48] and is the result of the charge localization on the small, spherical lithium cation which leads to the formation of clusters with the anions [49]. The calculated δ_η values are in the range for highly fragile glass-forming liquids as commonly found for ionic liquids [50]. A slight decrease for cyclic ammonium [FSI]$^-$ ionic liquids upon additions of [Li][FSI], similar to the findings for the aliphatic ammoniums here, has also been reported [51]. Since the investigated set of ionic liquids is quite similar in the structure and shows a comparable *T*-dependence, the activation energies of the viscous flow show the same trends as the values of the viscosity.
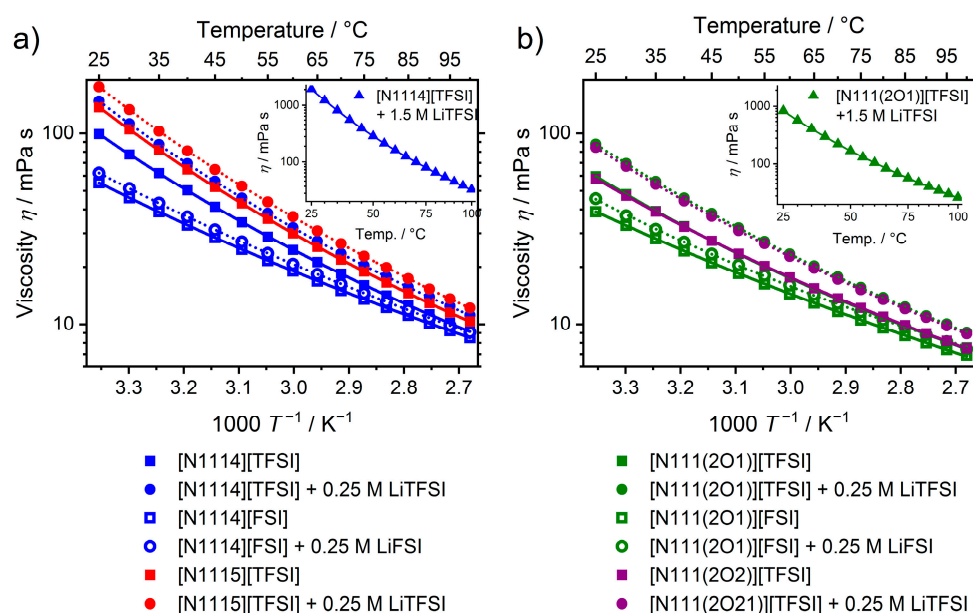

Figure 3. Temperature dependent viscosity for (**a**) the alkylated and (**b**) the ether substituted ionic liquids and mixtures with lithium salts. Lines are the corresponding VFT-fits. Drawn lines are for the pure ionic liquids, dashed ones for the mixtures with lithium salts.

3.3. Conductivity

Ionic liquids and solutions from these show an intrinsic ionic conductivity, which is essential for electrochemical devices. The conductivity of the battery electrolyte is one of the key factors limiting the current rate, and effects Ohmic losses and capacity. Number and mobility of the (unbound) charge carriers (ions) are thereby the factors that determine the obtained electrolyte conductivity. While ionic liquids have a high concentration of ions compared to the conventional carbonate electrolytes, they suffer from a lower mobility of the ions, which results from their higher viscosity. Altogether, ionic liquids usually have conductivities below those of the carbonate-based lithium electrolytes. This is mainly the result of the poorly shielded electrostatic interactions in the pure ionic liquid solutions, which lack coordinating molecules that are capable of separating the ions. Determining the conductivity of battery electrolytes is of central interest to understand the overall performance of electrolytes in electrochemical applications. The molar conductivities as calculated by Equation (1) and temperature-dependent parameters are given in Table 3. Experimental values for the *T*-dependent specific conductivity κ and fitting results are given in the supporting information.

Table 3. Calculated values of the molar conductivity Λ_M at 25 °C, parameters for the VFT fit, Angell strength factor δ_{Λ_M} and activation energy E_{a,Λ_M} (in the range of 25 to 60 °C) for the *T*-dependent molar conductivity.

Ionic Liquid	Li Salt c/mol·dm^{-3}	$\Lambda_M^{25\,°C}$/ S cm^2 mol^{-1}	$\Lambda_{M,0}$/ S cm^2 mol^{-1}	B_{Λ_M}/K	T_0/K	δ_{Λ_M}	E_{a,Λ_M} /kJ mol^{-1}
[N1114][TFSI]	-	0.567	197.2	−719.5	175.3	4.10	30.6
[N1114][TFSI]	0.25	0.377	234.5	−793.8	174.7	4.54	33.6
[N1114][TFSI]	1.5	0.025	199.2	−886.2	199.7	4.44	55.6
[N111(2O1)][TFSI]	-	0.874	203.4	−728.9	164.3	4.43	26.6
[N111(2O1)][TFSI]	0.25	0.623	173.6	−711.1	171.8	4.14	28.8
[N111(2O1)][TFSI]	1.5	0.067	192.3	−894.1	185.8	4.81	44.6
[N1114][FSI]	-	1.292	228.9	−786.3	146.3	5.37	22.9
[N1114][FSI]	0.25	1.105	175.7	−713.8	157.3	4.54	23.8
[N111(2O1)][FSI]	-	1.393	157.2	−675.0	155.3	4.35	22.0
[N111(2O1)][FSI]	0.25	1.240	177.9	−734.6	150.2	4.89	22.4
[N1115][TFSI]	-	0.409	177.1	−712.4	180.8	3.94	32.9
[N1115][TFSI]	0.25	0.277	199.3	−769.7	181.1	4.25	35.8
[N111(2O2)][TFSI]	-	0.849	189.4	−713.4	166.1	4.29	26.7
[N111(2O2)][TFSI]	0.25	0.591	239.9	−826.0	160.6	5.14	28.7

The molar conductivities at ambient temperature show the opposite trend than the viscosities, meaning that Λ_M increases when replacing [TFSI]$^-$ by [FSI]$^-$, CH$_2$ by oxygen, for shorter side-chains and with the addition of lithium salt. For the 1.5 M lithium solutions the molar conductivity at 25 °C is decreased by a factor of 22.7 ([N1114][TFSI]) and 13.0 ([N111(2O1)][TFSI]) compared to the pure ionic liquids. This difference decreases with temperature to a ratio of 5.2 ([N1114]$^+$) and 4.4 ([N111(2O1)]$^+$) at 85 °C. Temperature-dependent values of the molar conductivity follow the VFT-equation and show no crossover in the curves, Figure 4. The strength parameters δ_{Λ_M} again do not show clear trends and exhibit values in the interval from 3.94 to 5.37. The activation energy for the conductivity correlates with the activation energy for the viscous flow and shows the same trends as the values of the molar conductivity at 25 °C.
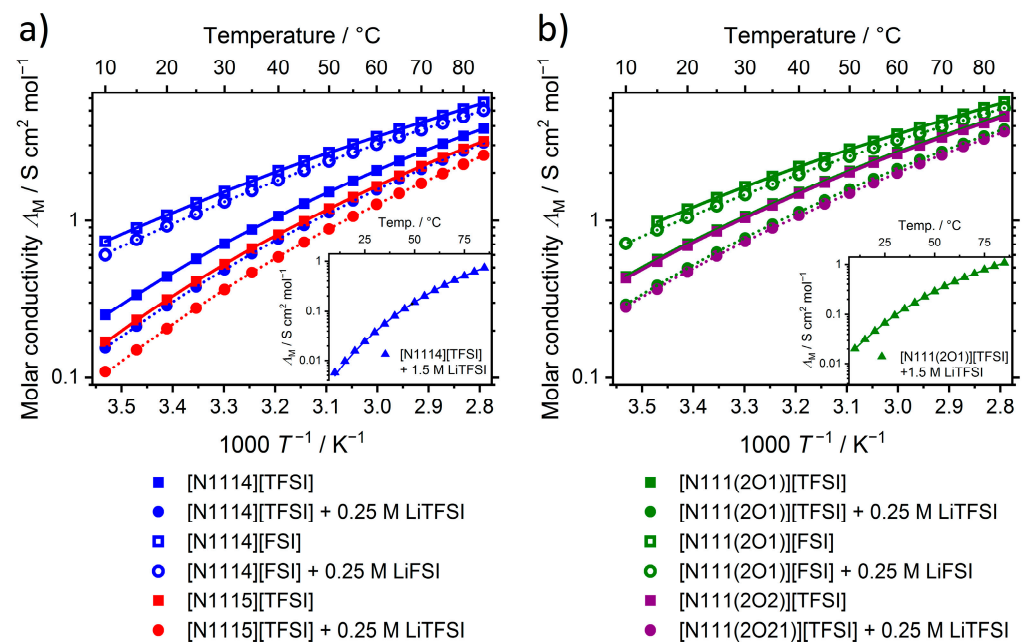

Figure 4. Temperature dependent molar conductivity for (**a**) the ionic liquids with alkyl and (**b**) ether side-chain. Lines are the corresponding VFT-fits. Drawn lines represent the pure ionic liquids, dashed ones are for the binary mixtures of ionic liquids and lithium salts.

The high similarities in the viscosity and conductivity trends of the pure ionic liquids and their salt mixtures are not unexpected, as ionic liquids are known to obey the Walden relation, Equations (5) and (6), thus their molar conductivity is inversely proportional to their viscosity.

$$\Lambda_M \propto \left(\eta^{-1} \right)^a \tag{5}$$

$$\log \Lambda_M = \log C + a \log \eta^{-1} \tag{6}$$

with the fractional exponent *a* close to unity and a constant *C*. Furthermore, the investigated samples have a high similarity in their molecular structure so that similar intermolecular forces and *T*-dependences of the transport properties can be expected. Walden plots are shown in Figure 5, parameters for the linear fit of Walden relation (5) are given in the supporting information.
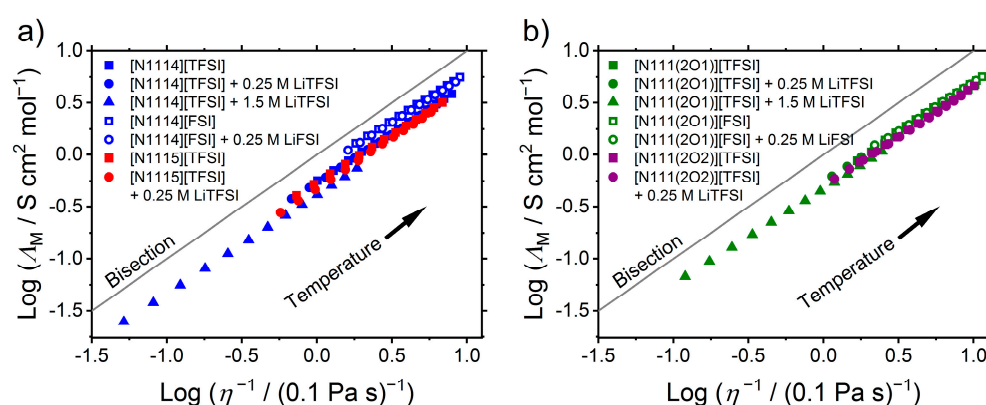

Figure 5. Walden plot of (**a**) the alkylated and (**b**) the ether-substituted ionic liquids showing the correlation of molar conductivity and inverse viscosity. The bisection of the Walden plot is often termed 'ideal KCl line' and the ionic liquids classified according to the difference from the bisection.

All values of the Walden exponent *a* lie in a quite small interval ranging from 0.915 to 0.966 as the chemical structures and interactions are quite similar. The [FSI]⁻ incorporating electrolytes are closer to the bisection (occasionally termed 'ideal KCl line' in the literature [52]). Addition of lithium salt causes an increase in distance to the bisection that is stronger for the alkylated samples and the electrolytes with higher [Li]⁺ concentration.

The decrease in molar conductivity upon addition of lithium salt to the ionic liquids can be understand in terms of formation of aggregates consisting of lithium cations and anions ([Li(A)$_x$]$^{1-x}$ with A being the anion of imide type), which reduce the overall amount of charge carriers [49,53]. Ether chains attached to cyclic ammonium cations were also shown to reduce the solvation number of anions per lithium cation [54]. This can be assumed to account for the finding that the dissolution of the lithium salts in the ionic liquids decreases the conductivity to a lower extent for the samples with ether functionalities and that these electrolytes deviate less form the pure species in the Walden plot. For similar ammonium ionic liquids with [TFSI]⁻, an activation energy in the same range is reported [15]. The finding that the exponent *a* of the Walden relation is smaller than 1 indicates that viscosity and molar conductivity do not show an ideal inverse relation [55]. Therefore, the result that the activation energies of the molar conductivities are slightly lower than for the viscosity is a necessary consequence and is also reported in the literature. The values for the ratio of the activation energy for molar conductivity to viscosity range from 0.907 to 0.968, which is similar to literature ranging from 0.898 to 0.947 [50].

3.4. Self-Diffusion Coefficients

As ionic liquids are composed of at least two constituents—cation and anion—the detailed knowledge of the individual contribution to the transport properties gives more detailed insight into structure–property-relations. These findings are of interest for both

fundamental investigations and optimizations when aiming at practical application. For the case of battery electrolytes, the transfer of the active species is the prerequisite for operating the batteries. Therefore, the transport mechanism and structuring of the active species is a central issue in electrolyte improvement. Measuring the self-diffusion coefficients of ionic liquid electrolytes by NMR spectroscopy gives access to the individual ion movements by addressing different nuclei or separated signals. Thus, a more detailed insight into the electrolyte is obtained than is accessible by measuring macroscopic transport properties such as viscosity and conductivity. In case of the ammonium ionic liquid, the self-diffusion coefficients $D_S(i)$ of species *i* were determined using the ^{1}H nucleus for the ionic liquid's cation, the ^{19}F nucleus for the anion and ^{7}Li for the lithium cation. Exemplary plots for the self-diffusion coefficients against reciprocal temperature are shown in Figure 6. Experimental values are listed in the supporting information.
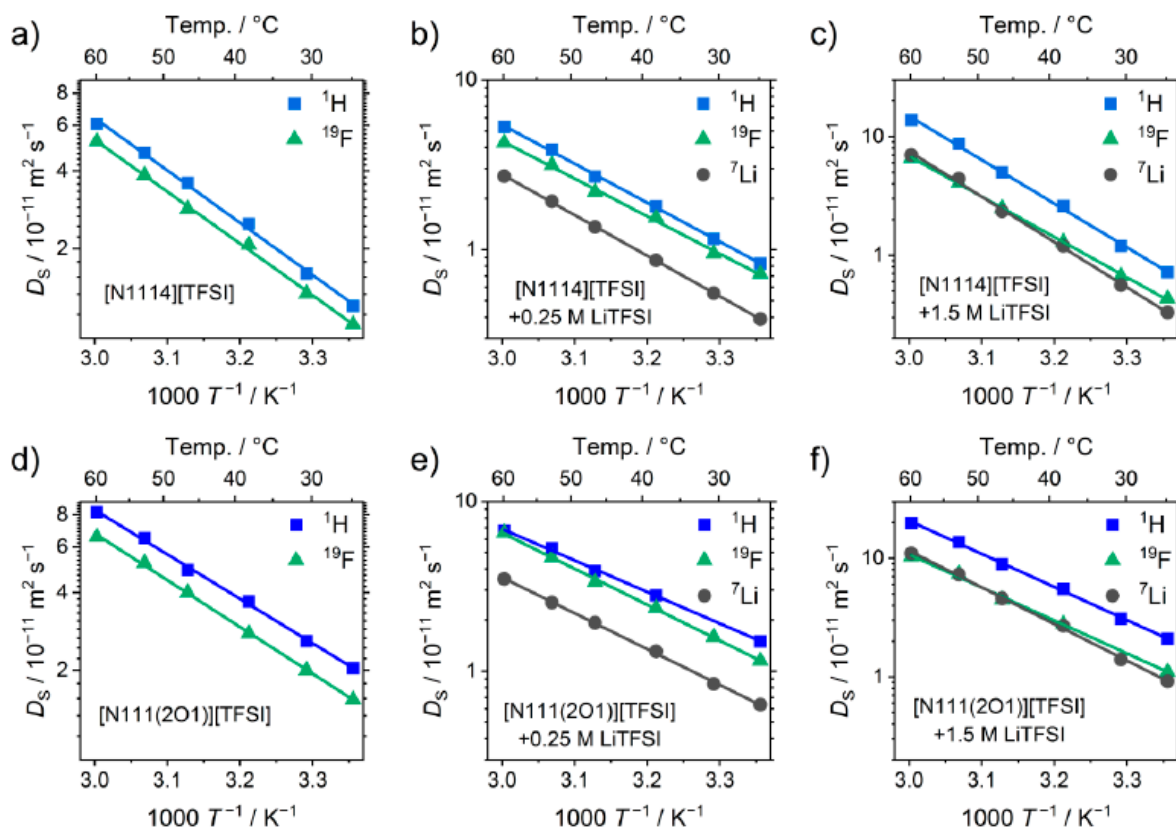

Figure 6. Exemplary plots of the *T*-dependent self-diffusion coefficients showing (**a–c**) the samples with the [N1114]$^+$ cation and (**d–f**) the samples with the [N111(2O1)]$^+$ cation with increasing Li-salt concentration. Given NMR-active nuclei correspond to the individual ions of the diffusing species (^{1}H: ionic liquid cation; ^{19}F: anion; ^{7}Li: lithium cation). Drawn lines are the linear fits following the Arrhenius Equation (4).

For the temperature-dependent self-diffusion coefficients, the general trend is that $D_S(^7\text{Li})$ is always smallest with exception of the 1.5 M samples at higher temperature where the diffusion of the lithium cation becomes slightly faster than the anions. For the samples with [TFSI]$^-$ the $D_S(^1\text{H})$ are always larger than $D_S(^{19}\text{F})$, while the situation is reversed for the electrolytes with [FSI]$^-$ anion. As the self-diffusion coefficients can be related to the other transport quantities by the Nernst–Einstein (NE) Equation (7) and Stokes–Einstein (SE) Equation (8) the same trends are found here.

$$\Lambda_{\text{M, NE}} = \frac{F^2}{RT} \sum_i \nu(i)\, z(i)^2\, D_S(i) \tag{7}$$

$$D_{\mathrm{S}}(i) = \frac{k_{\mathrm{B}}T}{\gamma\,\pi\,\eta\,\,r_{\mathrm{H}}(i)} \tag{8}$$

with $\Lambda_{\mathrm{M,\,NE}}$ the molar conductivity calculated by the NE equation, F the Faraday and R the universal gas constant, $\nu(i)$ the stochiometric coefficients and $z(i)$ the valences of ion i. k_{B} is the Boltzmann constant, γ a correction factor as the result of deviations from the assumption of the equations and the hydrodynamic boundary conditions, and $r_{\mathrm{H}}(i)$ is the hydrodynamic radius (Stokes radius) of the particle i [15,56,57]. It should be noted that these equations have some approximations in their derivation so that some care has to be taken in interpreting the results. The NE relation (6) was derived for ions in infinite dilution and the SE Equation (8) for large spherical particles without complex formation and interactions in a continuous medium. The factor γ is equal friction term of the (ideal) Stokes–Einstein equation and usually chosen to be $\gamma = 4$ (slip conditions) or $\gamma = 6$ (stick conditions) depending on the hydrodynamic boundary conditions. For pure ionic liquids it was shown that the slip conditions are a more appropriate description [58]. As the ideal assumptions for the SE equation are hardly met for molten salts, either in case of the pure ionic liquids or as binary solution with lithium salts, there are some controversies about their application towards the highly concentrated ionic systems [28,59,60]. Nevertheless, the relations are widely applied to ionic liquids and have proven useful to gain deeper insight into this substance class. The NE (7) and SE Equation (8) are therefore valuable for carving out trends of the interrelation between macroscopic properties essential for the application of ionic liquids and their molecular structure as realized by the synthetic chemist. As the macroscopic transport properties are linked to the microscopic ion movement, the trends of accelerated dynamics for samples with $[\mathrm{FSI}]^-$ anion, shorter side chains, cations with ether functionalization and lower $[\mathrm{Li}]^+$ concentration are also observed here. Activation energies for the self-diffusion (Table 4) follow these trends as well. Activation energies for the diffusion are higher than for the other transport processes following the order $E_{\mathrm{a},D_{\mathrm{S}}(i)} > E_{\mathrm{a},\eta} > E_{\mathrm{a},\Lambda_{\mathrm{M}}}$ without exceptions. It is striking that the activation energy of the self-diffusion coefficients is only slightly enlarged by lithium salt addition in the case of the $[\mathrm{FSI}]^-$ samples. The composition of the side chains seems to play only a minor role on the increase of the activation energy upon lithium addition, contrary to its influence on the activation energies for the pure ionic liquids. In general, the activation energies for the diffusion of the ionic liquid cation and anion are quite similar and lower than for the lithium cation. The only exception is the 0.25 M [N111(2O1)][FSI], where the lithium diffusion has the lowest activation energy.

Table 4. Activation energies of the self-diffusion for the ionic liquid cation (^{1}H), the common anion (^{19}F) and the lithium cation (^{7}Li) for bulk ionic liquids and their mixtures with lithium salts. Weighted activation energies $E_{\mathrm{a},D_{\mathrm{S}}(i)}$ are obtained by taking the stochiometric coefficients of the ions in mixtures into account. Values are obtained from Arrhenius fit in the T-range of 25–60 °C.

Ionic Liquid	Li Salt c/mol·dm^{-3}	$E_{\mathrm{a},D_{\mathrm{S}}(1\mathrm{H})}$ /kJ mol^{-1}	$E_{\mathrm{a},D_{\mathrm{S}}(19\mathrm{F})}$ /kJ mol^{-1}	$E_{\mathrm{a},D_{\mathrm{S}}(7\mathrm{Li})}$ /kJ mol^{-1}	$E_{\mathrm{a},D_{\mathrm{S}}(i)}$ /kJ·mol^{-1}
[N1114][TFSI]	-	38.8	38.4	-	38.6
[N1114][TFSI]	0.25	43.9	42.4	45.9	44.1
[N1114][TFSI]	1.5	70.6	65.2	73.1	68.7
[N111(2O1)][TFSI]	-	33.0	34.7	-	33.8
[N111(2O1)][TFSI]	0.25	35.6	40.5	40.4	40.3
[N111(2O1)][TFSI]	1.5	53.4	53.3	59.1	55.2
[N1114][FSI]	-	32.7	29.7	-	31.2
[N1114][FSI]	0.25	30.6	29.1	33.9	31.4
[N111(2O1)][FSI]	-	28.3	27.6	-	27.9
[N111(2O1)][FSI]	0.25	29.7	29.0	27.2	28.2
[N1115][TFSI]	-	43.3	38.8	-	41.0
[N1115][TFSI]	0.25	44.1	44.8	51.7	48.0
[N111(2O2)][TFSI]	-	34.5	33.8	-	34.2
[N111(2O2)][TFSI]	0.25	37.6	39.1	40.0	39.5

The diffusion activation energies increase upon doping a [TFSI]$^-$ ionic liquid with lithium salt, and similar activation energies were also reported in the literature [48]. Higher activation energies for the diffusion process than for the viscous flow are also observed even for quite different ionic liquids [28]. The ratio of the experimental molar conductivity, Λ_M, and the conductivity calculated by the Nernst–Einstein Equation (7) is often applied to analyze the low temperature molten salts. This ratio, which is the inverse of the Haven ration H_R, is often termed ionicity I_{HR} (Equation (9)) and is frequently interpreted as the amount of 'free ions' [61].

$$I_{HR} = (H_R)^{-1} = \frac{\Lambda_M}{\Lambda_{M,\,NE}} \tag{9}$$

In this model, it is assumed that the deviation of the measured conductivity from the Nernst–Einstein behavior has its origin in the formation of ion pairs or ion aggregates. The formation of such clusters of ions reduced the number of overall charge carriers [59]. Besides the dispute of the origin of the difference between the measured and calculated conductivities the quantification is still desired to gain a more detailed insight into the influence of structural elements. The *T*-dependent ionicity I_{HR}, Figure 7, decreased slightly with temperature.
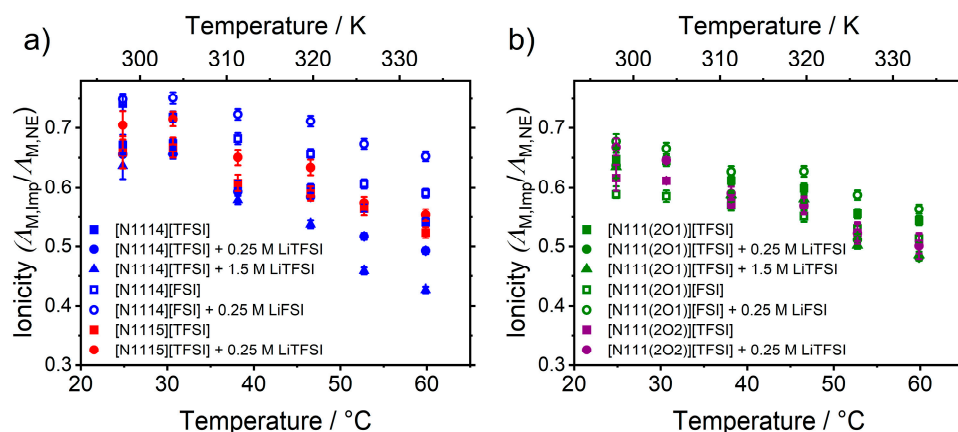

Figure 7. Temperature-dependent ionicity I_{HR} of the ionic liquids and mixtures with lithium salts for cations with (**a**) alkylated side chains and (**b**) attached ether-groups.

The samples with ether cations show a narrower distribution and slightly lower ionicity values. [FSI]$^-$ containing samples tend to higher values than those incorporating [TFSI]$^-$. This is consistent with literature findings for cyclic ammonium ionic liquids, where the [FSI]$^-$ samples showed higher ionicities than the [TFSI]$^-$ samples with the same cation and mild decreasing of I_{HR} for higher *T* [51,57]. A similar value ($I_{HR} \approx 0.6$) and minor change in the ionicity upon *T*-increase was also found for a pure ammonium [TFSI]$^-$ ionic liquid [15]. For phosphonium ionic liquids with hydrocarbon and ether functionalities, the ionicity also does not change significantly and addition of lithium salt leads to decreased I_{HR} values. Several literature results showed the existence of [Li(A)$_x$]$^{1-x}$ clusters for the imide-type ionic liquids as the interaction of the anion with the lithium cation is much stronger than with the ionic liquid cation [40,49,62,63]. These complexes would then reduce the amount of charge carriers, which would lead to a lower ionicity. Higher temperature is then expected to reduce the amount of aggregated species leading to higher ionicities. However, the contrary situation is observed here. Possible reasons for this may lie in a gradual change of the contribution of different transporting mechanisms, i.e., vehicular and structure diffusion mechanism [64], as seen in the concentration dependence of the lithium transfer [65]. Further investigations on the temperature-dependence of the lithium coordination and aggregation of ions might give further insight, if the ionicity interpretation can be related to the observed *T*-dependence. Other rationalizations of the ionicity, apart from the degree of unpaired ions, are for instance charge transfer form anion to cation [66] or

different diffusional states [67]. For pure ionic liquids, the deviation between experimental and Nernst–Einstein conductivity is frequently interpreted by velocity anti-correlations between the different ions [51].

Application of the Stokes–Einstein Equation (8) in the commonly used form is restricted since it contains two unknown parameters, the constant for the diffusion conditions γ and the Stokes radius $r_H(i)$. From the experimental data, only the product of the two parameters can be obtained, see Figure 8.
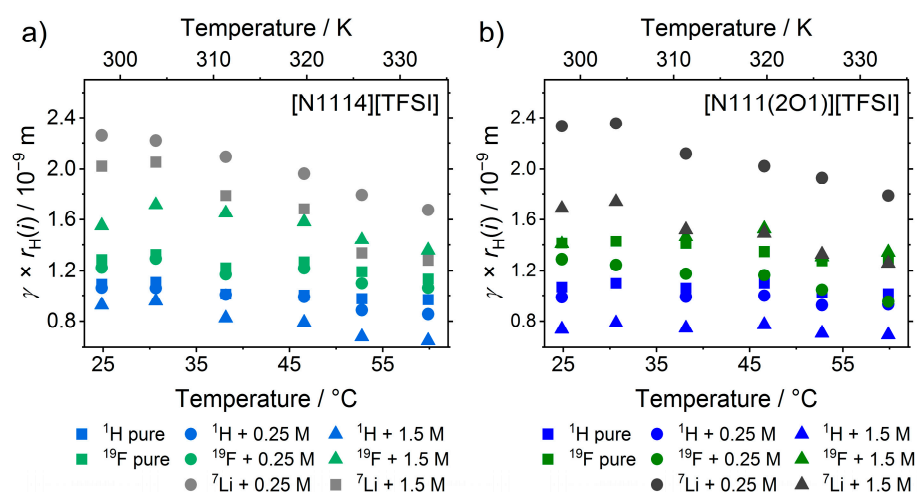
Figure 8. Exemplary plots of the product of Stokes radius and friction constant at different temperatures and different concentrations of [Li][TFSI] for (**a**) the [N1114]$^+$ and (**b**) the [N111(2O1)]$^+$ cation.

The values for $\gamma \times r_H(i)$ are always highest for the lithium cations with the exception of the 1.5 M samples at higher temperatures. For the [TFSI]$^-$ samples, the anions have higher values than the organic cations, whereas for the [FSI]$^-$ electrolytes the situation is inverted. The values are affected by temperature to a minor extent with a tendency of decreasing for higher temperatures and with higher effect on [Li]$^+$ ions. The findings of the lower $\gamma \times r_H(i)$ values for organic cations than for anions in samples with i = [TFSI]$^-$, and reversed situation in those with i = [FSI]$^-$, can be explained by the Van der Waals radius. For samples containing [TFSI]$^-$, the cations are smaller than the anion or comparable in size, leading to higher values of $\gamma \times r_H(i)$ for the anions [66]. The much higher $\gamma \times r_H(i)$ values for the small lithium cations are a clear indication of the formation of complexes with the anion if the same friction constant γ for all ions are proposed. The ion aggregation around [Li]$^+$ also explains the stronger decrease of $\gamma \times r_H(i)$ with temperature by the change in anion coordination or in the contributions of different diffusion mechanisms. Using the Van der Waals radii[62] from ab initio calculations as the Stokes radii in the Stokes–Einstein Equation (8) allows for the elimination of one unknown quantity [57]. In doing so, values for γ in the range of 3–4 are obtained for the organic cations and anions, whereas the lithium cations yielded constants from 19.4 to 42.6. This shows directly that the assumption of the Van der Waals radii of the ionic liquid ions is reasonable, whereas it is totally outrageous if non-coordinated lithium cations are supposed. Literature reports on ionic liquids revealed constants γ in the same range as observed in this study [15,28,56,57], thus deviating slightly from the values of the theoretical derivation.

It was investigated if aggregates of [Li]$_x$[IL]$_y$[anion]$_z$ structures can be identified by IR spectroscopy, although this was already described to be difficult with spectroscopy techniques [68]. Qualitatively it could be proved in case of [Li][TFSI] that a new IR absorption arises which is located at $581 − 582$ cm^{-1} (Figure 9). This absorption is in agreement with literature results and can be attributed to a Li-dimer structure [68]. Other absorption bands also reveal an interaction of complex structures (e.g., 571 cm^{-1} intensity, 522 cm^{-1} intensity). For [Li][FSI]-IL mixtures, a unique absorption peak in the 500–600 cm^{-1} region

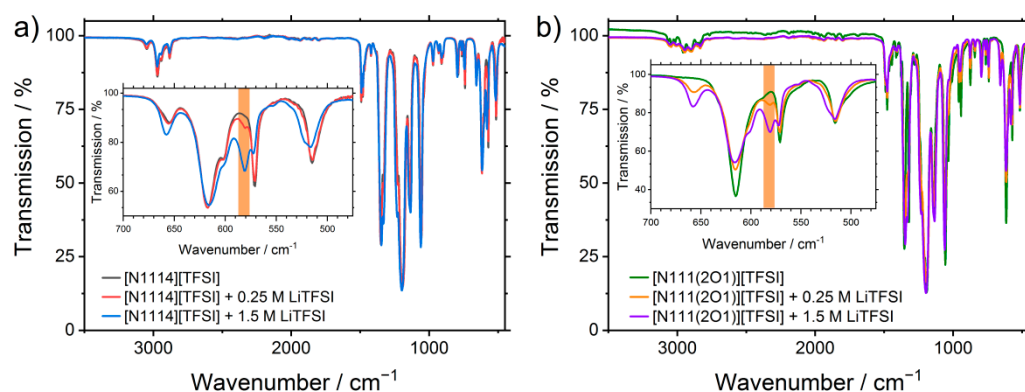was not observed. A week absorption at 592 cm^{-1} was observed in the case of [N1114][FSI] + [Li][FSI].

Figure 9. IR-spectra of the pure ionic liquids and their mixtures with (**a**) the alkylated cation [N1114]$^+$ and (**b**) the ether-substituted [N111(2O1)]$^+$ cation. Inserts show the area where the detection of complexes was reported in the literature.

3.5. Linear Sweep Voltammetry and Application in Li-ion Based Half-Cells

The oxidative stability of the ionic liquid–lithium imide salt mixtures were measured in blocking Pt electrode versus a lithium metal electrode configuration. A significant increase in current density implies the upper limit of the electrochemical window (ECW) of the electrolyte. Nevertheless, it should be considered that blocking electrodes may pretend to be too oxidative stable [69]. Table 5 summarizes the results with two different stability limit approaches, namely the current limit ($j = 50 \, \mu A \, cm^{-2}$) and the tangential approach.

Table 5. Summary of electrochemical stability (Pt vs. Li metal) and results of Li NMC half-cell test. The oxidative stability was determined by the current density (limit of 50 μA cm^{-2}) and the tangent approach at 1 mV s^{-1} within the first polarization to $U = 6.5$ V vs. Li/Li$^+$ at 25 °C. Li-ion cell tests with NMC (cathode) against Li (anode) electrodes in PAT-gas cell configuration from EL-Cell at $T = 60$ °C; Current rate = $C/20$ (CC/CC). Cell voltage range: 3.0 –4.3 V vs. Li/Li+. $C_{DC,n}$ is the discharge capacity of cycle n and C_t the theoretical capacity. It was not possible to cycle electrolyte [N111(2O1)][FSI] + [Li][FSI] more than one time (n.a.).

Ionic Liquid	Li Salt c/mol·dm^{-3}	E_{ox}/V $j = 50$ μAcm^{-2}	E_{ox}/V Tangent Approach	$C_{DC,2}$/ $C_{DC,1}$/%	$C_{DC,4}$/ $C_{DC,1}$/%	$C_{DC,2}$/ C_t/%	Lithium Plating
[N1114][TFSI]	-	>6.5	5.5	-	-	-	-
[N1114][TFSI]	0.25	5.5	5.2	100	100	84	yes
[N1114][TFSI]	1.5	5.5	5.3	-	-	-	-
[N111(2O1)][TFSI]	-	>6.5	>6.5	-	-	-	-
[N111(2O1)][TFSI]	0.25	>6.5	6.2	100	99	100	yes
[N111(2O1)][TFSI]	1.5	5.4	5.1	-	-	-	-
[N1114][FSI]	-	6.2	4.9	-	-	-	-
[N1114][FSI]	0.25	5.3	4.5	86	n.a.	98	yes
[N111(2O1)][FSI]	-	6.2	5.5	-	-	-	-
[N111(2O1)][FSI]	0.25	6.4	4.5	n.a.	n.a	n.a.	yes
[N1115][TFSI]	-	>6.5	5.4	-	-	-	-
[N1115][TFSI]	0.25	5.5	5.0	99	100	64	yes
[N111(2O2)][TFSI]	-	5.2	5.6	-	-	-	-
[N111(2O2)][TFSI]	0.25	5.3	5.2	99	95	86	yes

It can be observed that the ammonium based ionic liquids exhibit a wide oxidative stability window of $E_{ox} \geq 4.5$ V vs. Li/Li$^+$ even in case of [FSI]$^-$ anion salt at $T = 25$ °C. It is seen that the mixtures containing [TFSI]$^-$ anions show even greater stability of $E_{ox} \geq 5$ V vs. Li/Li$^+$. Due to the low current response, the current density approach may lead to systematic overestimation of the stability. However, for almost all systems, both approaches

for determining the oxidative limit (tangential approach/current density limit) result in comparable stability values. Ether containing side chains do not significantly reduce the E_{ox} values. In the tangential approach, it can be observed that the addition of lithium salt slightly reduces the E_{ox} values in the order of $0.2 - 1.5$ V. Overall, the compounds exhibit high oxidative stability, which makes them particularly suitable for use in high-voltage materials.

Cycling tests were performed in half-cell configuration (NMC versus Li electrodes) in EL-Cell "PAT-Cell-Press" including the pressure detection at $T = 60\,^{\circ}$C at $C/20$ current rate. Parameters were determined based on pre-tests of a selection of mixtures in coin cell configuration, cycled at different C-rates at $40\,^{\circ}$C. It was found that a current rate lower than 0.05 should be used due to the drop in capacitance at higher C-rates. A more serious issue here is that the relatively high viscosity and ion aggregate formation of the electrolytes can make Li transport into the NMC material difficult, even at high temperatures. Such harsh conditions at low current rates and high temperatures accelerate aging processes. Additionally, cycling against lithium avoids difficulties, which arise against graphite electrodes (e.g., intercalation of electrolyte components without additional additives). Usually the conducting salt concentration should be higher in cell tests; however, to ensure same composition as studied in depth above, we performed cell tests with low concentrated samples at reduced current rates. Cell data are shown in Supporting Information (Figure S2). The results of the cycling tests are shown in Table 5 as an overview and with more detail also in the Supporting Information (Tables S14 and S15).

During the cell tests, the internal pressure increases during the cycling (e.g., [N1114][TFSI] +0.25[Li][TFSI]), especially during charging periods. This might be an effect of gas formation and electrolyte decomposition during Li plating on newly created Li surface. A typical observed anode potential shifting around ± 20 mV can be observed for the mixture of [N1114][TFSI] with lithium salt. However, this charge-discharge jump is superimposed by a drift, which is clearly pronounced in some electrolytes (e.g., [N111(201)][TFSI] mixture or others in SI) up to hundreds of mV range. At the same time, the positive electrode (NMC) drifts correspondingly, which is, however, unexpected for such stable electrode materials. This led to the assumption that the drift is at least partly caused by a reaction of the reference electrode with the electrolyte, since the cathode is not expected to drift in this manner. Reactions with reference lithium electrodes like surface passivation or surface film formation can be accelerated by the temperature of $60\,^{\circ}$C. It is suggested that $[FSI]^-$ type salts are less stable than $[TFSI]^-$ type salts, which could be confirmed in this study, too. Overpotential values which are in the order of 60–180 mV, exhibit no clear trend between $[FSI]^-$ and $[TFSI]^-$ samples. It should be mentioned that for all electrolytes lithium plating was observed after disassembling which usually should be hindered in ionic liquid based electrolytes (cells were opened after discharging step). This can be attributed to both the low Li concentration, which induces fairly high internal cell resistances, and the relatively harsh cycling conditions overall for pure IL electrolytes.

High lithium (negative electrode)-to-lithium reference potential differences (namely considerable negative V2R values) indicate further an uncontrolled growth of lithium during lithium plating which accelerates also dendrite formation. In principle, however, the successful cycling suggests that the $[TFSI]^-$ containing electrolytes can be considered for cell testing, especially for the lower voltage LFP-based cells. Due to lithium plating, conclusions to Coulomb efficiency and capacity retention cannot be done in a reasonable manner. The initial cell experiments were intended to be a proof of concept, but systematic studies on cell experiments with feasible impedance measurements on interfacial effects are outside the scope of the manuscript. The exact mode of action will be shown in more detail in follow-up studies.

4. Conclusions

The structure–property relationships of various ionic liquid electrolytes with the trimethyl ammonium cation were investigated with particular focus on their applicability

in rechargeable lithium batteries. We investigated the influence of side chain length and composition, anion, and lithium concentration on the thermal and transport properties. The thermal transitions show a diverse behavior with crystalline phases for all samples with low lithium concentration, whereas samples with high lithium concentration formed glasses. The transport properties are comparable to other ionic liquid subclasses with accelerated dynamics for short side chains, ether functionalization, the use of the $[FSI]^-$ anion and low concentrations of lithium salt. The application of the Stokes–Einstein relation paired with IR-spectroscopy confirmed the formation of ion clusters or complexes involving the lithium cation, leading to slower dynamic of the lithium solutions compared to the bulk ionic liquids. It was shown that the ionic liquids exhibit a broad electrochemical window of > 4.5 V vs. Li/Li^+, which makes them suitable for high-voltage-applications. Half-cell tests against lithium metal at elevated temperatures showed better stability for TFSI-based salts than for FSI salts even if lithium plating was observed in all cell tests. In conclusion, it could be demonstrated that the novel ammonium based ionic liquids including [Li][TFSI] were able to successfully cycle NMC-Li cells at 60 °C.

Supplementary Materials: The following are available online at https://www.mdpi.com/article/10.3390/app11125679/s1: Synthesis of the ionic liquids and NMR resonances, experimental values for the transport properties, errors for data fitting, IR-spectra.

Author Contributions: Conceptualization, D.R. and A.H.; methodology, D.R. and A.H.; formal analysis, D.R. and A.H.; investigation, D.R., A.H. and T.Z.; resources, D.R.; writing—original draft preparation, D.R. and A.H.; writing—review and editing, D.R., A.H., F.P., C.W.M.K., T.Z., T.H. and R.H.; visualization, D.R. and A.H.; supervision, C.W.M.K. and T.H.; project administration, D.R. and A.H.; funding acquisition, C.W.M.K. All authors have read and agreed to the published version of the manuscript.

Institutional Review Board Statement: Not applicable.

Informed Consent Statement: Not applicable.

Data Availability Statement: Measured data points are given in the supporting information.

Conflicts of Interest: The authors declare no conflict of interest.

References

1. Welton, T. Ionic liquids: A brief history. *Biophys. Rev.* **2018**, *10*, 691–706. [CrossRef]
2. Singh, S.; Savoy, A.W. Ionic liquids synthesis and applications: An overview. *J. Mol. Liq.* **2020**, *297*, 112038. [CrossRef]
3. Watanabe, M.; Thomas, M.L.; Zhang, S.; Ueno, K.; Yasuda, T.; Dokko, K. Application of Ionic Liquids to Energy Storage and Conversion Materials and Devices. *Chem. Rev.* **2017**, *117*, 7190–7239. [CrossRef] [PubMed]
4. Gao, X.; Wu, F.; Mariani, A.; Passerini, S. Concentrated Ionic-Liquid-Based Electrolytes for High-Voltage Lithium Batteries with Improved Performance at Room Temperature. *ChemSusChem* **2019**, *12*, 4185–4193. [CrossRef] [PubMed]
5. Yang, Q.; Zhang, Z.; Sun, X.-G.; Hu, Y.-S.; Xing, H.; Dai, S. Ionic liquids and derived materials for lithium and sodium batteries. *Chem. Soc. Rev.* **2018**, *47*, 2020–2064. [CrossRef]
6. Navarra, M.A. Ionic liquids as safe electrolyte components for Li-metal and Li-ion batteries. *MRS Bull.* **2013**, *38*, 548–553. [CrossRef]
7. Hofmann, A.; Schulz, M.; Indris, S.; Heinzmann, R.; Hanemann, T. Mixtures of Ionic Liquid and Sulfolane as Electrolytes for Li-Ion Batteries. *Electrochim. Acta* **2014**, *147*, 704–711. [CrossRef]
8. Tsurumaki, A.; Agostini, M.; Poiana, R.; Lombardo, L.; Lufrano, E.; Simari, C.; Matic, A.; Nicotera, I.; Panero, S.; Navarra, M.A. Enhanced safety and galvanostatic performance of high voltage lithium batteries by using ionic liquids. *Electrochim. Acta* **2019**, *316*, 1–7. [CrossRef]
9. Wilken, S.; Xiong, S.; Scheers, J.; Jacobsson, P.; Johansson, P. Ionic liquids in lithium battery electrolytes: Composition versus safety and physical properties. *J. Power Sources* **2015**, *275*, 935–942. [CrossRef]
10. Osada, I.; De Vries, H.; Scrosati, B.; Passerini, S. Ionic-Liquid-Based Polymer Electrolytes for Battery Applications. *Angew. Chem. Int. Ed.* **2016**, *55*, 500–513. [CrossRef]

11. Sano, H.; Kitta, M.; Shikano, M.; Matsumoto, H. Effect of Temperature on Li Electrodeposition Behavior in Room-Temperature Ionic Liquids Comprising Quaternary Ammonium Cation. *J. Electrochem. Soc.* **2019**, *166*, A2973–A2979. [CrossRef]

12. Ruether, T.; Bhatt, A.I.; Best, A.S.; Harris, K.R.; Hollenkamp, A.F. Electrolytes for Lithium (Sodium) Batteries Based on Ionic Liquids: Highlighting the Key Role Played by the Anion. *Batter. Supercaps* **2020**, *3*, 793–827. [CrossRef]

13. Jeong, S.; Li, S.; Appetecchi, G.B.; Passerini, S. Asymmetric ammonium-based ionic liquids as electrolyte components for safer, high-energy, electrochemical storage devices. *Energy Storage Mater.* **2019**, *18*, 1–9. [CrossRef]

14. Shkrob, I.A.; Marin, T.W.; Zhu, Y.; Abraham, D.P. Why Bis(fluorosulfonyl)imide Is a "Magic Anion" for Electrochemistry. *J. Phys. Chem. C* **2014**, *118*, 19661–19671. [CrossRef]

15. Hayamizu, K.; Tsuzuki, S.; Seki, S. Transport and Electrochemical Properties of Three Quaternary Ammonium Ionic Liquids and Lithium Salts Doping Effects Studied by NMR Spectroscopy. *J. Chem. Eng. Data* **2014**, *59*, 1944–1954. [CrossRef]

16. Balducci, A. Ionic Liquids in Lithium-Ion Batteries. *Top. Curr. Chem.* **2017**, *375*, 20. [CrossRef]

17. Xiao, J. How lithium dendrites form in liquid batteries. *Science* **2019**, *366*, 426–427. [CrossRef]

18. Xu, W.; Wang, J.; Ding, F.; Chen, X.; Nasybulin, E.N.; Zhang, Y.; Zhang, J.-G. Lithium metal anodes for rechargeable batteries. *Energy Environ. Sci.* **2014**, *7*, 513–537. [CrossRef]

19. Cheng, X.-B.; Zhang, R.; Zhao, C.-Z.; Zhang, Q. Toward Safe Lithium Metal Anode in Rechargeable Batteries: A Review. *Chem. Rev.* **2017**, *117*, 10403–10473. [CrossRef]

20. Liu, K.; Wang, Z.; Shi, L.; Jungsuttiwong, S.; Yuan, S. Ionic liquids for high performance lithium metal batteries. *J. Energy Chem.* **2021**, *59*, 320–333. [CrossRef]

21. Liu, B.; Zhang, J.-G.; Xu, W. Advancing Lithium Metal Batteries. *Joule* **2018**, *2*, 833–845. [CrossRef]

22. Tikekar, M.D.; Choudhury, S.; Tu, Z.; Archer, L.A. Design principles for electrolytes and interfaces for stable lithium-metal batteries. *Nat. Energy* **2016**, *1*, 16114. [CrossRef]

23. Hu, M.; Pang, X.; Zhou, Z. Recent progress in high-voltage lithium ion batteries. *J. Power Sources* **2013**, *237*, 229–242. [CrossRef]

24. Xu, W.; Cooper, E.I.; Angell, C.A. Ionic Liquids: Ion Mobilities, Glass Temperatures, and Fragilities. *J. Phys. Chem. B* **2003**, *107*, 6170–6178. [CrossRef]

25. Wang, X.; Chi, Y.; Mu, T. A review on the transport properties of ionic liquids. *J. Mol. Liq.* **2014**, *193*, 262–266. [CrossRef]

26. Harris, K.R.; Kanakubo, M. Self-Diffusion Coefficients and Related Transport Properties for a Number of Fragile Ionic Liquids. *J. Chem. Eng. Data* **2016**, *61*, 2399–2411. [CrossRef]

27. Sippel, P.; Lunkenheimer, P.; Krohns, S.; Thoms, E.; Loidl, A. Importance of liquid fragility for energy applications of ionic liquids. *Sci. Rep.* **2015**, *5*, 13922. [CrossRef] [PubMed]

28. Green, S.M.; Ries, M.E.; Moffat, J.; Budtova, T. NMR and Rheological Study of Anion Size Influence on the Properties of Two Imidazolium-based Ionic Liquids. *Sci. Rep.* **2017**, *7*, 1–12. [CrossRef] [PubMed]

29. Calvar, N.; Domínguez, Á. Thermal Behaviour of Pure Ionic Liquids. In *Ionic Liquids Current State of the Art*; IntechOpen: London, UK, 2015; pp. 199–208.

30. Girard, G.M.A.; Hilder, M.; Zhu, H.; Nucciarone, D.; Whitbread, K.; Zavorine, S.; Moser, M.; Forsyth, M.; MacFarlane, D.R.; Howlett, P.C. Electrochemical and physicochemical properties of small phosphonium cation ionic liquid electrolytes with high lithium salt content. *Phys. Chem. Chem. Phys.* **2015**, *17*, 8706–8713. [CrossRef]

31. Le, M.L.P.; Tran, N.A.; Ngo, H.P.K.; Nguyen, T.G.; Tran, V.M. Liquid Electrolytes Based on Ionic Liquids for Lithium-Ion Batteries. *J. Solut. Chem.* **2015**, *44*, 2332–2343. [CrossRef]

32. Galiński, M.; Lewandowski, A.; Stępniak, I. Ionic liquids as electrolytes. *Electrochimica Acta* **2006**, *51*, 5567–5580. [CrossRef]

33. Sangoro, J.R.; Kremer, F. Charge Transport and Glassy Dynamics in Ionic Liquids. *Accounts Chem. Res.* **2012**, *45*, 525–532. [CrossRef]

34. Armel, V.; Velayutham, D.; Sun, J.; Howlett, P.C.; Forsyth, M.; Macfarlane, D.R.; Pringle, J.M. Ionic liquids and organic ionic plastic crystals utilizing small phosphonium cations. *J. Mater. Chem.* **2011**, *21*, 7640–7650. [CrossRef]

35. Yunis, R.; Al-Masri, D.; Hollenkamp, A.F.; Doherty, C.M.; Zhu, H.; Pringle, J.M. Plastic Crystals Utilising Small Ammonium Cations and Sulfonylimide Anions as Electrolytes for Lithium Batteries. *J. Electrochem. Soc.* **2020**, *167*, 070529. [CrossRef]

36. Philippi, F.; Rauber, D.; Zapp, J.; Präsang, C.; Scheschkewitz, D.; Hempelmann, R. Multiple Ether-Functionalized Phosphonium Ionic Liquids as Highly Fluid Electrolytes. *ChemPhysChem* **2019**, *20*, 443–455. [CrossRef]

37. Philippi, F.; Rauber, D.; Kuttich, B.; Kraus, T.; Kay, C.W.M.; Hempelmann, R.; Hunt, P.A.; Welton, T. Ether functionalisation, ion conformation and the optimisation of macroscopic properties in ionic liquids. *Phys. Chem. Chem. Phys.* **2020**, *22*, 23038–23056. [CrossRef]

38. Martinelli, A.; Matic, A.; Jacobsson, P.; Börjesson, L.; Fernicola, A.; Scrosati, B. Phase Behavior and Ionic Conductivity in Lithium Bis(trifluoromethanesulfonyl)imide-Doped Ionic Liquids of the Pyrrolidinium Cation and Bis(trifluoromethanesulfonyl)imide Anion. *J. Phys. Chem. B* **2009**, *113*, 11247–11251. [CrossRef] [PubMed]

39. Bayley, P.M.; Best, A.S.; Macfarlane, D.R.; Forsyth, M. Transport Properties and Phase Behaviour in Binary and Ternary Ionic Liquid Electrolyte Systems of Interest in Lithium Batteries. *ChemPhysChem* **2011**, *12*, 823–827. [CrossRef] [PubMed]

40. Kerner, M.; Plylahan, N.; Scheers, J.; Johansson, P. Ionic liquid based lithium battery electrolytes: Fundamental benefits of utilising both TFSI and FSI anions? *Phys. Chem. Chem. Phys.* **2015**, *17*, 19569–19581. [CrossRef]

41. Angell, C. Perspective on the glass transition. *J. Phys. Chem. Solids* **1988**, *49*, 863–871. [CrossRef]

42. Araque, J.C.; Hettige, J.J.; Margulis, C.J. Modern Room Temperature Ionic Liquids, a Simple Guide to Understanding Their Structure and How It May Relate to Dynamics. *J. Phys. Chem. B* **2015**, *119*, 12727–12740. [CrossRef] [PubMed]

43. Tsuzuki, S.; Hayamizu, K.; Seki, S. Origin of the Low-Viscosity of [emim][(FSO2)2N] Ionic Liquid and Its Lithium Salt Mixture: Experimental and Theoretical Study of Self-Diffusion Coefficients, Conductivities, and Intermolecular Interactions. *J. Phys. Chem. B* **2010**, *114*, 16329–16336. [CrossRef]

44. Triolo, A.; Russina, O.; Caminiti, R.; Shirota, H.; Lee, H.Y.; Santos, C.S.; Murthy, N.S.; Castner, J.E.W. Comparing intermediate range order for alkyl- vs. ether-substituted cations in ionic liquids. *Chem. Commun.* **2012**, *48*, 4959–4961. [CrossRef]

45. Russina, O.; Triolo, A.; Gontrani, L.; Caminiti, R.; Xiao, D.; Jr, L.G.H.; A Bartsch, R.; Quitevis, E.L.; Pleckhova, N.; Seddon, K.R. Morphology and intermolecular dynamics of 1-alkyl-3-methylimidazolium bis{(trifluoromethane)sulfonyl}amide ionic liquids: Structural and dynamic evidence of nanoscale segregation. *J. Physics Condens. Matter* **2009**, *21*, 424121. [CrossRef]

46. Shimizu, K.; Bernardes, C.E.S.; Triolo, A.; Lopes, J.N.C. Nano-segregation in ionic liquids: Scorpions and vanishing chains. *Phys. Chem. Chem. Phys.* **2013**, *15*, 16256–16262. [CrossRef] [PubMed]

47. Chen, Z.; Huo, Y.; Cao, J.; Xu, L.; Zhang, S. Physicochemical Properties of Ether-Functionalized Ionic Liquids: Understanding Their Irregular Variations with the Ether Chain Length. *Ind. Eng. Chem. Res.* **2016**, *55*, 11589–11596. [CrossRef]

48. Hayamizu, K.; Tsuzuki, S.; Seki, S.; Ohno, Y.; Miyashiro, H.; Kobayashi, Y. Quaternary Ammonium Room-Temperature Ionic Liquid Including an Oxygen Atom in Side Chain/Lithium Salt Binary Electrolytes: Ionic Conductivity and1H,7Li, and19F NMR Studies on Diffusion Coefficients and Local Motions. *J. Phys. Chem. B* **2008**, *112*, 1189–1197. [CrossRef] [PubMed]

49. Castiglione, F.; Famulari, A.; Raos, G.; Meille, S.V.; Mele, A.; Appetecchi, G.B.; Passerini, S. Pyrrolidinium-Based Ionic Liquids Doped with Lithium Salts: How Does Li+ Coordination Affect Its Diffusivity? *J. Phys. Chem. B* **2014**, *118*, 13679–13688. [CrossRef]

50. Schreiner, C.; Zugmann, S.; Hartl, R.; Gores, H.J. Temperature Dependence of Viscosity and Specific Conductivity of Fluoroborate-Based Ionic Liquids in Light of the Fractional Walden Rule and Angell's Fragility Concept†. *J. Chem. Eng. Data* **2010**, *55*, 4372–4377. [CrossRef]

51. Rüther, T.; Kanakubo, M.; Best, A.S.; Harris, K.R. The importance of transport property studies for battery electrolytes: Revisiting the transport properties of lithium–N-methyl-N-propylpyrrolidinium bis(fluorosulfonyl)imide mixtures. *Phys. Chem. Chem. Phys.* **2017**, *19*, 10527–10542. [CrossRef]

52. Harris, K.R. On the Use of the Angell–Walden Equation To Determine the "Ionicity" of Molten Salts and Ionic Liquids. *J. Phys. Chem. B* **2019**, *123*, 7014–7023. [CrossRef]

53. Giffin, G.A.; Moretti, A.; Jeong, S.; Pilar, K.; Brinkkötter, M.; Greenbaum, S.G.; Schönhoff, M.; Passerini, S.; Brinkkoetter, M.; Greenbaum, S.; et al. Connection between Lithium Coordination and Lithium Diffusion in [Pyr 12O1][FTFSI] Ionic Liquid Electrolytes. *ChemSusChem* **2018**, *11*, 1981–1989. [CrossRef]

54. Shimizu, M.; Yamaguchi, K.; Usui, H.; Ieuji, N.; Yamashita, T.; Komura, T.; Domi, Y.; Nokami, T.; Itoh, T.; Sakaguchi, H. Piperidinium-Based Ionic Liquids as an Electrolyte Solvent for Li-Ion Batteries: Effect of Number and Position of Oxygen Atom in Cation Side Chain on Electrolyte Property. *J. Electrochem. Soc.* **2020**, *167*, 070516. [CrossRef]

55. Yamaguchi, T.; Yonezawa, T.; Koda, S. Study on the temperature-dependent coupling among viscosity, conductivity and structural relaxation of ionic liquids. *Phys. Chem. Chem. Phys.* **2015**, *17*, 19126–19133. [CrossRef] [PubMed]

56. Tokuda, H.; Hayamizu, K.; Ishii, K.; Susan, M.A.B.H.; Watanabe, M. Physicochemical Properties and Structures of Room Temperature Ionic Liquids. 2. Variation of Alkyl Chain Length in Imidazolium Cation. *J. Phys. Chem. B* **2005**, *109*, 6103–6110. [CrossRef]

57. Hayamizu, K.; Tsuzuki, S.; Seki, S.; Fujii, K.; Suenaga, M.; Umebayashi, Y. Studies on the translational and rotational motions of ionic liquids composed of N-methyl-N-propyl-pyrrolidinium (P13) cation and bis(trifluoromethanesulfonyl)amide and bis(fluorosulfonyl)amide anions and their binary systems including lithium salts. *J. Chem. Phys.* **2010**, *133*, 194505. [CrossRef]

58. Schmidt, J.R.; Skinner, J.L. Hydrodynamic boundary conditions, the Stokes–Einstein law, and long-time tails in the Brownian limit. *J. Chem. Phys.* **2003**, *119*, 8062–8068. [CrossRef]

59. Nordness, O.; Brennecke, J.F. Ion Dissociation in Ionic Liquids and Ionic Liquid Solutions. *Chem. Rev.* **2020**, *120*, 12873–12902. [CrossRef]

60. Harris, K.R. Relations between the Fractional Stokes−Einstein and Nernst−Einstein Equations and Velocity Correlation Coefficients in Ionic Liquids and Molten Salts. *J. Phys. Chem. B* **2010**, *114*, 9572–9577. [CrossRef]

61. Ueno, K.; Tokuda, H.; Watanabe, M. Ionicity in ionic liquids: Correlation with ionic structure and physicochemical properties. *Phys. Chem. Chem. Phys.* **2010**, *12*, 1649–1658. [CrossRef] [PubMed]

62. Tong, J.; Wu, S.; Von Solms, N.; Liang, X.; Huo, F.; Zhou, Q.; He, H.; Zhang, S. The Effect of Concentration of Lithium Salt on the Structural and Transport Properties of Ionic Liquid-Based Electrolytes. *Front. Chem.* **2020**, *7*, 1–10. [CrossRef]

63. Figueiredo, P.H.; Siqueira, L.; Ribeiro, M.C.C. The Equilibrium Structure of Lithium Salt Solutions in Ether-Functionalized Ammonium Ionic Liquids. *J. Phys. Chem. B* **2012**, *116*, 12319–12324. [CrossRef] [PubMed]

64. Li, Z.; Smith, G.D.; Bedrov, D. Li+ Solvation and Transport Properties in Ionic Liquid/Lithium Salt Mixtures: A Molecular Dynamics Simulation Study. *J. Phys. Chem. B* **2012**, *116*, 12801–12809. [CrossRef] [PubMed]

65. Brinkkötter, M.; Mariani, A.; Jeong, S.; Passerini, S.; Schönhoff, M. Ionic Liquid in Li Salt Electrolyte: Modifying the Li + Transport Mechanism by Coordination to an Asymmetric Anion. *Adv. Energy Sustain. Res.* **2021**, *2*, 2000078. [CrossRef]

66. Philippi, F.; Quinten, A.; Rauber, D.; Springborg, M.; Hempelmann, R. Density Functional Theory Descriptors for Ionic Liquids and the Introduction of a Coulomb Correction. *J. Phys. Chem. A* **2019**, *123*, 4188–4200. [CrossRef]

67. Feng, G.; Chen, M.; Bi, S.; Goodwin, Z.A.H.; Postnikov, E.B.; Brilliantov, N.; Urbakh, M.; Kornyshev, A.A. Free and Bound States of Ions in Ionic Liquids, Conductivity, and Underscreening Paradox. *Phys. Rev. X* **2019**, *9*, 021024. [CrossRef]
68. Lassègues, J.-C.; Grondin, J.; Aupetit, C.; Johansson, P. Spectroscopic Identification of the Lithium Ion Transporting Species in LiTFSI-Doped Ionic Liquids. *J. Phys. Chem. A* **2009**, *113*, 305–314. [CrossRef]
69. Hofmann, A.; Werth, F.; Höweling, A.; Hanemann, T. Investigation of the Oxidative Stability of Li-Ion Battery Electrolytes Using Cathode Materials. *ECS Electrochem. Lett.* **2015**, *4*, A141–A144. [CrossRef]